ФИЗИКА ЭЛЕМЕНТАРНЫХ ЧАСТИЦ И АТОМНОГО ЯДРА
2003. Т. 34. ВЫП. 6

УДК 539;1 546.02

MICROSCOPIC NUCLEAR MODELS AND NUCLEAR DATA FOR ASTROPHYSICS

I. N. Borzov, S. Goriely

Institut d'Astronomie et d'Astrophysique, Universite Libre de Bruxelles, Bruxelles

ФИЗИКА ЭЛЕМЕНТАРНЫХ ЧАСТИЦ И АТОМНОГО ЯДРА
2003. Т. 34. ВЫП. 6

УДК 539;1 546.02

MICROSCOPIC NUCLEAR MODELS AND NUCLEAR DATA FOR ASTROPHYSICS

I. N. Borzov, S. Goriely

Institut d'Astronomie et d'Astrophysique, Universite Libre de Bruxelles, Bruxelles

Although an important effort has been devoted in the last decades to the measurement of the decay half-lives and reaction cross sections, major astrophysics applications, such as the nucleosynthesis of the heavy elements, involve so many exotic nuclei for which so many different properties need to be known that only theoretical predictions can fill the gaps. For nucleosynthesis applications, the nuclear ingredients to the reaction or weak interaction models should preferentially be estimated from microscopic global predictions based on sound and reliable nuclear models which, in turn, can compete with more phenomenological highly-parametrized models in the reproduction of experimental data. The latest developments made in deriving the nuclear inputs of relevance in astrophysics applications are reviewed. It mainly concerns nuclear structure properties (atomic masses, deformations, radii, etc.), nuclear level densities, nucleon- and α-nucleus optical potentials, γ-ray and β-decay strength functions. Emphasis is made on the possibility of making use of reliable microscopic models for practical applications.

Хотя в последние десятилетия много усилий было посвящено измерению времен жизни и сечений реакций, основные астрофизические приложения, такие как нуклеосинтез тяжелых элементов, включают так много экзотических ядер с большим количеством свойств, которые необходимо знать, что только теоретические предсказания могут дать необходимую информацию. В приложении к нуклеосинтезу ядерные компоненты в реакционных моделях и моделях слабого взаимодействия должны, главным образом, оцениваться согласно микроскопическим глобальным предсказаниям, основанным на надежных и проверенных ядерных моделях, которые, в свою очередь, могут конкурировать в описании экспериментальных данных с феноменологическими моделями, использующими огромное количество параметров. Обзор посвящен новейшим достижениям, полученным при выводе ядерных компонент, имеющих значение в астрофизических приложениях. Они, главным образом, связаны со свойствами ядерной структуры (атомные массы, деформации, радиусы и т. д.), плотностью ядерных уровней, нуклонно- и α-ядерным оптическим потенциалами, γ-лучевой и β-распадной силовыми функциями. Акцент делается на возможности использования достоверных микроскопических моделей на практике.

INTRODUCTION

Nuclear astrophysics is a vastly interdisciplinary field. There is a large number of different physical problems invoked calling for a variety of different and complementary research fields (for a review, see [1, 2]). Impressive progress has been made for the last decades in the various fields related to nuclear astrophysics. Factors contributing to these rapid developments include progress in experimental and theoretical nuclear physics, as well as in ground-based or space astronomical

observations and astrophysical modellings. In spite of that success, major problems and puzzles remain, which challenge continuously the nuclear astrophysics concepts and findings. To put them on a safer footing requires in particular a deeper and more precise understanding of the many nuclear physics processes operating in the astrophysical environment. Among the numerous objectives in nuclear astrophysics, let us mention some major issues:

• the nature, structure, composition and evolution of objects such as low- and intermediate-mass stars, massive stars, supernovae of type I or II, white dwarfs, neutron stars, novae, X-ray bursts, γ-ray bursts, ...

• the nucleosynthesis of elements lighter than iron, and in particular species like ^{3}He, ^{7}Li, ^{15}N, ^{19}F, ^{23}Na, ^{26}Al, in low- and intermediate-mass stars, massive stars, novae, supernovae of type I or II, ...

• the nucleosynthesis of elements heavier than iron by

— the slow neutron-capture process (or s process) in low- and intermediate-mass AGB stars and massive stars,

— the rapid neutron-capture process (or r process) possibly, in exploding massive stars or neutron star mergers, and

— the p process in the oxygen/neon layers at the presupernova stage or during the stellar explosion of massive stars.

All these questions raise major nuclear challenges that up to now have been addressed in a more or less satisfactory way. Astrophysics needs in nuclear data are defined by the astrophysics modelling and by the sensitivity of the astrophysics predictions to the nuclear input. Depending on the level of reliability of the astrophysics model, a relevant answer about the impact of nuclear uncertainties on the astrophysics observables can be given. Our ability to model astrophysics sites varies with the complexity to describe numerically the corresponding physical mechanisms. Schematically, four classes of models can be defined according to their level of reliability: (i) state-of-the-art 3-D self-consistent parameters-free models, (ii) realistic self-consistent 1-D models, (iii) parametrized (semirealistic) 1-D models and (iv) phenomenological fully-parametric site-independent models. Nowadays, almost no astrophysics simulation is performed on the basis of 3-D self-consistent models, and as regards nuclear uncertainties, not a single study has ever been made in such refined calculations. Major modelling difficulties still need to be solved, in particular in the description of convection, radiation and neutrino transport, plasma equation of state, mass loss by stars, rotation and magnetic effects, ... For this reason, in all the still-open nuclear astrophysics questions, nuclear physics must be regarded as a necessary, but not a sufficient condition to solve the problems. This fundamental issue should be kept in mind when estimating the importance of nuclear physics for astrophysical applications. Extensive studies about the impact of nuclear physics, for example, on nonexplosive H- and He-burning phases can be found in [3], explosive nucleosynthesis in type II

supernovae in [4], s-process nucleosynthesis in [5–7], r-process nucleosynthesis in [8–10], nucleo-cosmochronometry in [11–13], p-process nucleosynthesis in [10, 14–16].

Strong, weak and electromagnetic interaction processes play an essential role in nuclear astrophysics (for a review, see [2]). Nuclear reactions concern thermonuclear as well as spallation reactions. The thermonuclear reactions taking place in stars include the capture of nucleons or α particles at relatively low energies (far below 1 MeV for neutrons and the Coulomb barrier for charged particles). They are of pivotal importance for the stellar energy balance, as well as for the bulk composition of the galaxies and for the peculiar abundances observed at the surface of stars of certain classes. The spallation reactions act in low temperature and density media through the interaction of particles (nonthermally) accelerated up to energies in excess of some tens of MeV per nucleon with the interstellar medium, or with the material (gas or grains) at stellar surfaces or in circumstellar shells. β-decay rates, as well as electron or positron captures are also fundamental for our understanding of specific scenarios in stellar evolution (e. g., presupernova and supernova models) and nucleosynthesis (e. g., the r process). Although important effort has been devoted in the last decades to measure decay half-lives and reaction cross sections, major difficulties related to the specific conditions of the astrophysical plasma remain, and only theoretical predictions can fill the gaps. Charged-particle induced reactions at stellar energies (far below the Coulomb barrier) have cross sections that are not too low to be measured at the present time. Stellar reactions often concern unstable or even exotic (neutron-rich, neutron-deficient, superheavy) species for which no experimental data exist. Given astrophysical applications (e. g., the r or p processes of nucleosynthesis) involve a large number (thousands) of unstable nuclei for which many different properties have to be determined (including ground and excited state properties, strong, weak and electromagnetic interaction properties). In high-temperature environments, thermalization effects of excited states by electron or photon interactions, as well as ionization effects significantly modifies the nuclear properties in a way that it remains difficult or almost impossible to simulate in the laboratory. For example, electron screening in the laboratory conditions complicates the experimental determination of the bare cross section characterizing the ionized stellar environments. The contribution of thermally populated excited states, as well as atomic effects in the strongly ionized stellar plasma can modify by orders of magnitude the laboratory β-decay and electron capture half-lives. Finally, in high-density environments, the basic definition of the nucleus is lost and nuclear binding must be understood in terms of a nuclear equation of state. For all these specificities found in astrophysical plasmas, theoreticians are requested to supply reliable determination of all relevant quantities to the experimentally unreachable energy and mass regions. For some specific applications (e. g., the r process), almost no experimental data are available at all.

To fulfill these specific requirements, when estimating the different nuclear inputs for astrophysics applications, two major features of the nuclear theory must be contemplated, namely its *microscopic* and *universal* aspect. A microscopic description by a physically sound model based on first principles ensures a reliable extrapolation away from experimentally known region. On the other hand, a universal description of all nuclear properties within one unique framework for all nuclei involved ensures a coherent prediction of all unknown data. For these reasons, when the nuclear ingredients to the reaction (e. g., Hauser–Feshbach) or weak interaction (e. g., the Quasiparticle Random Phase Approximation or QRPA) models cannot be determined from experimental data, use is made preferentially of microscopic or semimicroscopic global predictions based on sound and reliable nuclear models which, in turn, can compete with more phenomenological highly-parametrized models in the reproduction of experimental data. The selection criterion of the adopted model is fundamental, since most of the nuclear ingredients in rate calculations need to be extrapolated in an energy and mass domain out of reach of laboratory measurements, where parametrized systematics based on experimental data can fail drastically. Global microscopic approaches have been developed for the last decades but almost never used for practical applications, because of their lack of accuracy in reproducing experimental data, especially when considered globally on a large data set. On the other hand, as we defined the astrophysical models according to their reliability, different classes of nuclear models can be contemplated, starting from local macroscopic approaches up to global microscopic approaches. We find in between these two extremes, approaches like the classical (e. g., liquid drop, droplet), semi-classical (e. g., Thomas–Fermi), macroscopic-microscopic (e. g., classical with microscopic corrections), semimicroscopic (e. g., microscopic with phenomenological corrections) and fully microscopic (e. g., mean field, shell model, self-consistent QRPA) approaches. Characterizing the earlier stages of the microscopic models history, it could be stated in a very schematic way that the higher the degree of sophistication, the less accurate the model reproduced the bulk set of experimental data. The classical or phenomenological approaches are highly parametrized and therefore often successful in reproducing experimental data, or at least they have been much more accurate than microscopic calculations. The lower accuracy obtained with microscopic models has originated both from their deficiencies and computational complications making the determination of free parameters by fits to experimental data time-consuming. This reliability vs accuracy character of nuclear theories is detailed below for most of the relevant quantities needed to estimate reaction or β-decay rates, namely nuclear masses, nuclear level densities, optical potentials, γ-ray and β-decay strength functions. Nowadays, the status of the consistently microscopic models is gradually changing, as they have achieved a mature state of development. They also can be tuned at the same level of accuracy as the phenomenological models, and therefore could replace

the phenomenological inputs little by little in practical applications. The needs for further theoretical investigations in each of these fields are also stressed in the following sections.

1. GLOBAL MICROSCOPIC MODELS FOR REACTION RATE CALCULATIONS

1.1. Reaction Models. Various models have been developed in order to complement the experimental information on reaction cross section when necessary. Concerning reactions on light species, the microscopic cluster model, based on a first-principle approach, has become an established tool to perform the necessary extrapolations at the low energies of relevance in astrophysics. In that model, the nucleons are grouped into clusters. Keeping the internal cluster degrees of freedom fixed, the totally antisymmetrized relative wave functions between the various clusters are determined by solving the Schrödinger equation for a many-body Hamiltonian with an effective nucleon-nucleon interaction. When compared with most others, this approach has the major advantage of providing a consistent, unified and successful description of the bound, resonant, and scattering states of a nuclear system. The microscopic cluster model remains superior to other frequently used extrapolation procedures. It has been applied to many astrophysically important reactions involving light systems, and been very successful in determining low-energy cross sections. Despite these successes, more effort in that direction are obviously needed.

As far as reaction on heavier nuclei are concerned, most of the cross-section calculations for nucleosynthesis applications are based on the statistical model of Hauser–Feshbach [17, 18]. Such a model makes the fundamental assumption that the capture process takes place with the intermediary formation of a compound nucleus in thermodynamic equilibrium. The energy of the incident particle is then shared more or less uniformly by all the nucleons before releasing the energy by particle emission or γ deexcitation. The formation of a compound nucleus is usually justified by assuming that the level density in the compound nucleus at the projectile incident energy is large enough to ensure an average statistical continuum superposition of available resonances. However, when the number of available states in the compound system is relatively small, the validity of the Hauser–Feshbach predictions has to be questioned, the capture process being possibly dominated by direct electromagnetic transitions to a bound final state rather than through a compound nucleus intermediary. Direct reactions are known to play an important role for light or closed shell systems for which no resonant states are available. It has also been shown through a simple analytical model [19] that the direct capture contribution may dominate the statistical contribution for heavy neutron-magic targets with low enough neu-

tron binding energy. The direct neutron capture rates have been systematically estimated for all exotic neutron-rich nuclei produced by the r process [9]. The corresponding direct capture rates are calculated within a microscopic model based on the neutron potential of [20] and making use of the excited level spectrum in the residual nucleus predicted by a combinatorial model of nuclear level densities [21]. The resulting single-particle configuration is assumed to be characterized by an average spectroscopic factor as infered from systematics based on experimental (d, p) reactions. In this approach, the direct capture rates are found to be proportional to the number of levels of energy lower than the neutron binding energy. Consequently, the direct capture mechanism is often not negligible compared with the compound nucleus process for nuclei close to the valley of stability. Neutron-rich nuclei present direct capture rates which show large variations according to the allowed or forbidden $E1$ transitions available between the initial and final systems. The direct capture model still suffers from large uncertainties stemming essentially from the predicted excitation spectrum of the residual nucleus. This includes the energy, spin, parity and spectroscopic factors of all the levels below the neutron binding energy. A full knowledge of these quantities is required to improve the predictive power of the direct capture model. More experimental data as well as improved microscopic models are requested.

Both the direct and statistical models have proven their ability to predict cross sections accurately. However, these models suffer from uncertainties stemming essentially from the predicted nuclear ingredients describing the nuclear structure properties of the ground and excited states, and the strong and electromagnetic interaction properties. Clearly, the knowledge of the ground state properties (masses, deformations, matter densities) of the target and residual nuclei is indispensable. When not available experimentally, this information has to be obtained from nuclear mass models. The excited state properties have also to be known. Experimental data may be scarce above some excitation energy, and especially so for nuclei located far from the valley of nuclear stability. This is why frequent resort to a level density prescription is mandatory. In the Hauser–Feshbach formalism, the probability for particle emission is calculated by solving the Schrödinger equation with the appropriate optical potential for the particle-nucleus interaction. Finally, the electromagnetic de-exciation of the compound nucleus is calculated assuming the dominance of dipole $E1$ transitions (the $M1$ transitions are usually included as well, but do not contribute significantly. They will not be discussed further here). As schematized in Fig. 1, phenomenological, as well as microscopic models are available for each of these ingredients. Nowadays, microscopic models can be tuned at the same level of accuracy as the phenomenological models, renormalized on experimental data if needed. The nuclear models available today to estimate all these nuclear ingredients are described below.

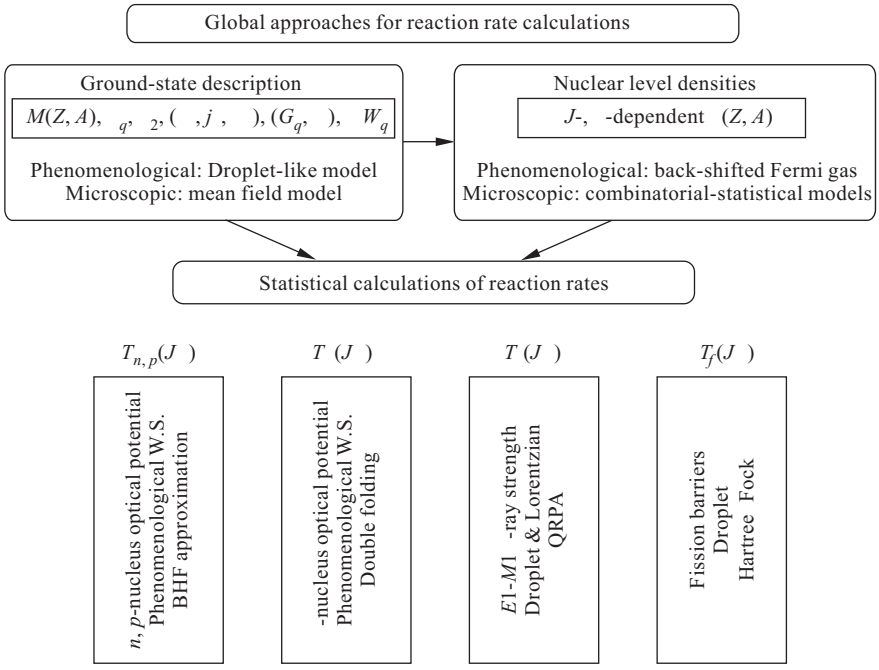

Fig. 1. Global phenomenological and microscopic theories used to estimate the ground- and excited state properties, as well as transmission coefficients T of relevance in the Hauser–Feshbach model. Details are given in the text

1.2. Prediction of Ground State Properties. Among the ground state properties, the atomic mass $M(Z, A)$ is obviously the most fundamental quantity and enters all chapters of nuclear astrophysics. Their knowledge is indispensable to estimate the rate and energetics of any nuclear transformation. Although masses for more than about 2000 nuclei are known experimentally [22,23], important nuclear astrophysics applications, like the r or p processes, involve exotic neutron-rich and neutron-deficient nuclei for which no experimental data exist. The calculation of the reaction and decay rates also requires the knowledge of other ground state properties, such as the deformation, density distribution, single-particle level scheme, pairing force, shell correction energies, ... for which nuclear structure theory must provide predictions. The impact of the different mass models on the r- and p-processes predictions is discussed, for example, in [10].

Attempts to develop formulas estimating the nuclear masses of nuclei go back to the 1935 «semi-empirical mass formula» of von Weizsäcker [24]. Being

inspired by the liquid-drop model of the nucleus, this is the macroscopic mass formula *par excellence*. Improvements have been brought little by little to the original mass formula, leading to the development of macroscopic-microscopic mass formulas [25], where microscopic corrections to the liquid drop part are introduced in a phenomenological way. In this framework, the macroscopic and microscopic features are treated independently, both parts being connected exclusively by a parameter fit to experimental masses. Later developments included in the macroscopic part properties of infinite and semi-infinite nuclear matter and the finite range character of nuclear forces. Until recently the atomic masses were calculated on the basis of one form or another of the liquid-drop model, the most sophisticated version of which is the «finite-range droplet model» (FRDM) [26]. Despite the great empirical success of this formula (it fits the 1888 $Z \geq 8$ masses with an r. m. s. error of 0.689 MeV), it suffers from major shortcomings, such as the incoherent link between the macroscopic part and the microscopic correction, the instability of the mass prediction to different parameter sets, or the instability of the shell correction. There is an obvious need to develop, for astrophysics applications, a mass formula that is more closely connected to the basic nuclear interactions [10]. Two such approaches can reasonably be contemplated at the present time, one being the non-relativistic Hartree–Fock (HF) method; and the other, the relativistic Hartree method, also known as the relativistic mean-field (RMF) method. Progress in the HF and RMF mass models has been slow, presumably because of the computer-time limitations that arose in the past with deformed nuclei. Nuclear forces are traditionally determined by fitting to the masses (and some other properties) of less than ten or so nuclei. The resulting forces give rise to r. m. s. deviations from the 1888 experimental masses [22] well in excess of 2 MeV. This is far from reaching the level of precision found by droplet-like models (around 0.7 MeV).

The result is that the most microscopically founded mass formulas of practical use were till recently those based on the so-called ETFSI (extended Thomas–Fermi plus Strutinsky integral) method [27]. The ETFSI method is a high-speed approximation to the HF method based on Skyrme forces, with pairing correlations generated by a δ-function force that is treated in the usual BCS approach. In the latest version of the ETFSI mass model (ETFSI2), eleven parameters are found to reproduce the 1719 experimental masses of the $A \geq 36$ nuclei with an r. m. s. deviation of 0.709 MeV [28] comparable with the one obtained with the droplet-like formula. The ETFSI model remains an approach of the macroscopic-microscopic type, although it provides a high degree of coherence between the macroscopic and microscopic terms through the unifying Skyrme force underlying both parts. A logical step towards improvements obviously consists in considering now the HF method as such. It was demonstrated very recently [29, 30] that HF calculations in which a Skyrme force is fitted to essentially all the mass data are not only feasible, but can also compete with the most accurate droplet-like

formulas available nowadays. Such HF calculations are based on the conventional Skyrme force of the form

$$v_{ij} = t_0(1 + x_0P_\sigma)\delta(\mathbf{r}_{ij}) + t_1(1 + x_1P_\sigma)\frac{1}{2\hbar^2}\{p_{ij}^2\delta(\mathbf{r}_{ij}) + \text{h. c.}\} + \\ + t_2(1 + x_2P_\sigma)\frac{1}{\hbar^2}\mathbf{p}_{ij}\delta(\mathbf{r}_{ij})\mathbf{p}_{ij} + \frac{1}{6}t_3(1 + x_3P_\sigma)\rho^\gamma\delta(\mathbf{r}_{ij}) + \\ + \frac{i}{\hbar^2}W_0(\boldsymbol{\sigma_i} + \boldsymbol{\sigma_j})\mathbf{p}_{ij} \times \delta(\mathbf{r}_{ij})\mathbf{p}_{ij}, \quad (1)$$

and a δ-function pairing force acting between like nucleons,

$$v_{\text{pair}}(\boldsymbol{r}_{ij}) = V_{\pi q}\ \delta(\boldsymbol{r}_{ij}), \quad (2)$$

in which the density independent zero range pairing force is characterized by a strength parameter $V_{\pi q}$ allowed to be different for neutrons and protons, and also to be slightly stronger for an odd number of nucleons ($V_{\pi q}^-$) than for an even number ($V_{\pi q}^+$), i. e., the pairing force between neutrons, for example, depends on whether N is even or odd. Both mass formulas add to the energy corresponding to the above force the Coulomb energy and a phenomenological Wigner term of the form

$$E_W = V_W \exp\left\{-\lambda\left(\frac{N-Z}{A}\right)^2\right\} + V'_W|N-Z|\exp\left\{-\left(\frac{A}{A_0}\right)^2\right\}. \quad (3)$$

The first competing HFBCS mass table (in which the pairing interaction is treated in the BCS approximation) was obtained with the MSk7 Skyrme and pairing parameters which were determined by fitting to the full data set of 1719 $A \geq 36$ masses [22] with a final r. m. s. error of 0.702 MeV.

In the case of the highly neutron-rich nuclei that are of particular interest in the context of the r process, the validity of the BCS approach to pairing is questionable. The BCS procedure neglects the fact that the scattering of nucleon pairs between different single-particle states under the influence of the pairing interaction will actually modify the single-particle states, a difficulty that becomes particularly serious close to the neutron-drip line, where nucleon pairs will be scattered into the continuum. For such nuclei, this problem is avoided in the HF–Bogoliubov (HFB) method, which puts the pairing correlations into the variational function, so that the single-particle and pairing aspects are treated simultaneously and on the same footing. Lately [31, 32], a new Skyrme force has been derived on the basis of HF calculations with pairing correlations taken into account in the Bogoliubov approach, using a δ-function pairing force. The r. m. s. error with respect to the masses of all the 2135 measured nuclei of the 2001 Audi & Wapstra compilation [23] with $Z, N \geq 8$ is 0.674 MeV (see Fig. 2). The quality of the new predictions is similar to the one obtained with HFBCS.

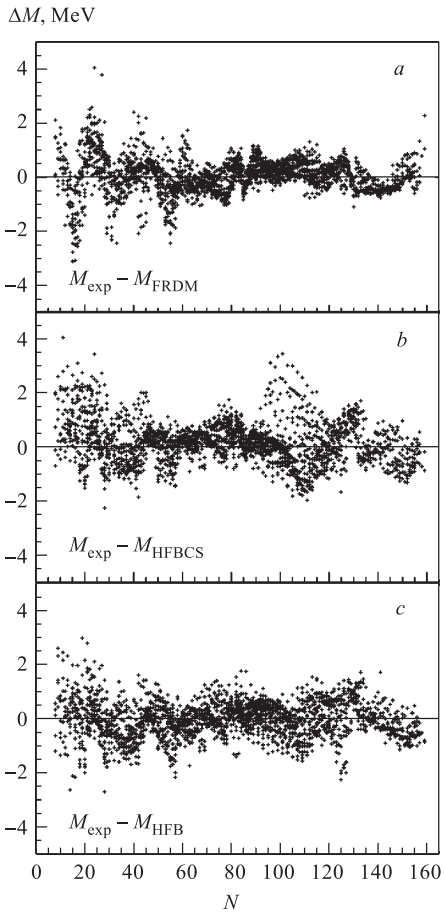

Fig. 2. Comparison between measured masses [23] and the predictions of three mass models: *a*) FRDM [26]; *b*) FBCS [30]; *c*) HFB [32]

The complete mass table, HFB-2, has been constructed, giving all nuclei lying between the two drip lines over the range $Z, N \geq 8$ and $Z \leq 120$. A comparison between HFB and HFBCS masses shows that the HFBCS model is a very good approximation to the HFB theory, in particular for masses, the extrapolated masses never differing by more than 2 MeV below $Z \leq 110$. The reliability of the predictions far away from the experimentally known region, and in particular towards the neutron drip line, is however increased thanks to the improved treatment of the pairing correlations. Figure 3 provides a comparison between the HFB and FRDM predictions. It demonstrates vividly that two mass models which reproduce measured masses with comparable r. m. s. deviations can diverge more or less markedly in their predictions for nuclei far from stability. It should also be noted that, even if the HFB and FRDM mass parabolas present more or less the same slope, they sometimes differ noticeably in their predicted deformations or shell structures. These differences may have a significant impact on nucleosynthesis predictions.

Although complete mass tables have now been derived within the HFB approach, further developments that could have an impact on mass extrapolations towards the neutron drip line are still needed. Unsatisfactory feature of the present schemes is the use of nonuniversal parametrization of pairing force in the fitting procedure. (More generally, it has been argued in [33] that the present calculations of the nuclear masses are not able to reproduce the chaotic components of the nucleons motion which may be due to particular effective interactions.) The changes within the Skyrme–HFB approach may be those associated with making the pairing force density-dependent within the Lipkin–Nogami

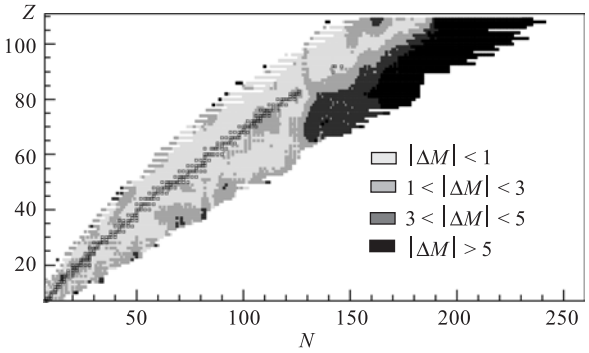

Fig. 3. Mapping of the chart of the nuclides in the ranges N and $Z \geq 8$, and $Z \leq 110$ with the differences $\Delta M = M_{\mathrm{HFB}} - M_{\mathrm{FRDM}}$ between the HFB and FRDM theoretical predictions. The differences are coded as indicated in the figure

prescription. More fundamentally, mean field models need to be improved, so that all possible observables (such as giant dipole, Gamow–Teller excitations, nuclear matter properties) can be estimated coherently on the basis of one unique energy-density functional or effective NN interaction. For example, empirical values of the nucleonic effective mass or the Landau–Migdal parameters can be in contradiction with the values deduced from the existing forces. In particular, adding a t_4 term to the Skyrme force (with a density and momentum dependent term) is likely to reconcile the large nucleonic mass required to fit masses with nuclear matter calculations [34].

Let us briefly mention the main approaches alternative to the ones employing the zero-range Skyrme-like forces and finite-range Gogny forces. They are based on different energy density functionals and effective Lagrangians. The relativistic mean field approach incorporates a phenomenologic meson-nucleon Lagrangian. In the application to nuclear ground state masses, the relativistic Hartree formalism with static meson fields has been used augmented by no-sea approximation in nucleon sector (see [35]). The masses of measured nuclei are described typically with the r. m. s. error of about 2 MeV (no readjustment of the parameters has been made). The extrapolation behavior is strikingly different from that of FRDM and ETFSI models.

The quasiparticle Lagrangian model [36,37] which is an extension of Landau–Migdal quasiparticle concept takes into account the first order energy dependence of the nucleon mass operator and constrains imposed by self-consistent criteria [38]. The energy dependence of the effective NN interaction results in shifting the position of the neutron drip-line to substantially larger values of

neutron-excess than the ones given by phenomenological energy-density functionals with the energy-independent interactions.

The effective quasiparticle local energy-density functional (EDF) approach (see [39] and Refs. therein) is based on the existence theorem by Hohenberg and Kohn [40] and Kohn–Sham quasiparticle formalism. In the latest version of the EDF proposed in [41], the volume part is fitted by fractional expression to the equation of state (EOS) of the pure neutron matter [42] and symmetric nuclear matter [43] up to the density $\rho \approx 1$ fm^{-3}. The extrapolation of EOS to higher densities preserves casuality. In inhomogeneous system, a surface part of the EDF is to describe the finite-range and nonlocal in-medium effects via Padé approximant for unknown expansion containing density gradients [41]. In addition to the usual Coulomb direct and exchange interaction energies, an effective ρ-dependent Coulomb-nuclear correlation term is included to cure the Nolen–Schiffer anomaly. The method allows one to describe the experimental masses for about 100 spherical nuclei with the r. m. s. deviation of 1.2 MeV with no readjustment of the parameters. The extrapolation of the masses to the drip lines locates between the ETFSI and FRDM predictions.

Concomitantly, shell model calculations (e. g., in the quantum Monte Carlo approach) provide further fundamental insight on the nuclear ground state properties of exotic nuclei. The well-known shell-model mass formulae [44] based on the Hamiltonian consisting of the phenomenological monopole term plus realistic NN interaction and containing 28 parameters gives the fit to 1751 binding energies for $N, Z \geq 8$ with r. m. s. error of 375 keV. The recent shell model calculations have also shown that the spin-isospin dependent part of the effective NN interaction in nuclei could lead to a change of the magic numbers $N = 8, 20$ in the exotic neutron-rich region [45]. These effects are probably underestimated in Skyrme–Hartree–Fock calculations because the interaction is truncated to be of the δ-function type. Future global shell-model calculations will certainly reveal interesting properties of heavier exotic neutron-rich nuclei. As has been mentioned above, the various nuclear aspects are extremely complicate to reconcile within one unique framework. Thus, the quest towards universality will most certainly be the focus of fundamental nuclear physics research for the coming decade.

1.3. Nuclear Level Densities. As for the determination of the nuclear ground state properties, until recently, only classical approaches were used to estimate nuclear level densities (NLD) for practical applications (see [46]). Although reliable microscopic models (in the statistical and combinatorial approaches) have been developed for the last four decades, the back-shifted Fermi gas model (BSFG) approximation — or some variant of it — remains the most popular approach to estimate the spin-dependent NLD, particularly in view of its ability to provide a simple analytical formula (e. g., [47,48]). Although numerous parametrizations of the BSFG formula are available today, only few propose a global formula applica-

ble to the whole nuclear chart. One such efficient parametrization is given here as an example (see [49] for more details). It corresponds to the classical BSFG approximation of the state density $\rho(U)$ and level density $\rho(U,J)$ of a nucleus (Z,A) with a given angular momentum J and excitation energy U, i. e.,

$$\rho(U) = \frac{\sqrt{\pi}}{12a^{1/4}(U-\delta)^{5/4}} \times \times \mathrm{e}^{2\sqrt{a(U-\delta)}}, \quad (4)$$

$$\rho(U,J) = \frac{2J+1}{2\sqrt{2\pi}\sigma^3}\rho(U) \times \times \mathrm{e}^{-(J+1/2)^2/2\sigma^2}, \quad (5)$$

where microscopic (shell, pairing and deformation) corrections to the binding energy are introduced in the U-dependent NLD parameter a by the approximation [48]

$$a(U) = = \tilde{a}[1 + 2\gamma E_{\mathrm{mic}}\,\mathrm{e}^{-\gamma(U-\delta)}]. \quad (6)$$

The microscopic energy $E_{\mathrm{mic}} = E_{\mathrm{tot}}(Z,A) - E_{\mathrm{LD}}$ is derived from the experimental (or theoretical) binding energy $E_{\mathrm{tot}}(Z,A)$ and the simple spherical liquid drop formula

$$E_{\mathrm{LD}} = a_v A + a_s A^{2/3} + + (a_{\mathrm{sym}} + a_{ss}A^{-1/3})AI^2 + + a_c\frac{Z^2}{A^{1/3}}, \quad (7)$$

where $I = (N-Z)/A$. A fit to the 1888 $N,Z \geq 8$ experimental masses [22] (with a final r. m. s. deviation of only 3 MeV) leads to the liquid drop parameters (in MeV): $a_v = -15.6428$, $a_s = 17.5418$, $a_{\mathrm{sym}} = 27.9418$, $a_{ss} = -25.3440$, and $a_c = 0.70$. Concerning the NLD parameters, a fit to the experimental s-neutron resonance spacings [47] gives $\tilde{a} = 0.101A + 0.036A^{2/3}$ (MeV^{-1}),

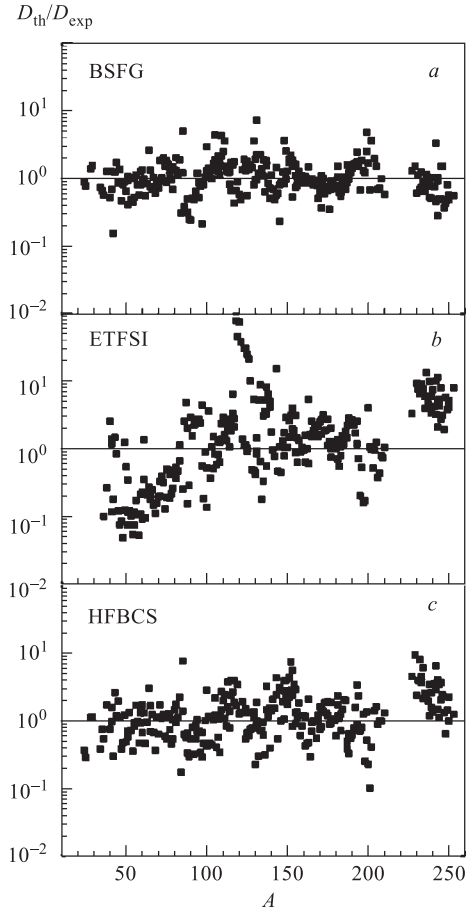

Fig. 4. Comparison between experimental s-wave neutron resonance spacings D_{exp} at the neutron separation energy S_n and predicted values D_{th} derived from the use of the ETFSI [48] (*b*) or of a HFBCS [52] (*c*) model. The results from the global BSFG approximation of [49] are also shown (*a*)

$\gamma = 0.03$, $\sigma^2 = 0.0194A^{5/3}\sqrt{U/a}$, and $\delta = 0.5$, 0, -0.5 MeV for even–even, odd–mass, and odd–odd nuclei, respectively. As shown in Fig. 4, this global parametrization predicts experimental resonance spacings with a high degree of accuracy [49].

However, it is often forgotten that the BSFG model essentially introduces phenomenological improvements to the original analytical formulation of Bethe, and consequently none of the important shell, pairing, and deformation effects are properly accounted for in such a description. Drastic approximations are usually made in deriving analytical formulae and often their shortcomings in matching experimental data are overcome by empirical parameter adjustments. It is well accepted that the shell correction to the NLD cannot be introduced by neither an energy shift, nor a simple energy-dependent level density parameter, and that the complex BCS pairing effect cannot be reduced to an odd–even energy back-shift (e. g., [48]). This shortcoming is cured to some extent by adjustments of a more or less large number of free parameters. Such a procedure introduces, however, a substantial unreliability if predictions have to be made when experimental data are scarce or nonexistent, as it is very often the case in certain, sometimes extended, ranges of excitation energies, or for nuclei far from stability of importance for the modeling of the p process and for a large variety of other applications. The lack of measured level densities still constitutes the main problem faced by the NLD models and the parameter fitting procedures they require, even if the number of analyses of slow neutron resonances and of cumulative numbers of low energy levels grows steadily. This concerns in particular the s-wave neutron resonance spacings D at the neutron separation energy S_n. For a nucleus $(Z, A{+}1)$ resulting from the capture of a low-energy neutron by a target (Z, A) with spin J_0, D is given by

$$\begin{aligned} D &= \frac{2}{\rho(S_n, J_0 + 1/2) + \rho(S_n, J_0 - 1/2)} \quad \text{for } J_0 > 0, \\ D &= \frac{2}{\rho(S_n, 1/2)} \qquad\qquad\qquad\qquad\quad \text{for } J_0 = 0, \end{aligned} \tag{8}$$

the factor of 2 in the numerator relating to the classical assumption of equal probabilities of both parities π at all energies.

Several approximations used to obtain the NLD expressions in an analytical form can be avoided by quantitatively taking into account the discrete structure of the single-particle spectra associated with realistic average potentials [50]. In this approach, the intrinsic J-independent level density is expressed as

$$\omega(U) = \frac{\mathrm{e}^{S(U)}}{(2\pi)^{3/2}\sqrt{D(U)}} \tag{9}$$

and the T-dependent entropy S and excitation energy U are derived from the summation on the doubly degenerate single-particle levels ε_q^k (with blocking effect for odd nucleon systems)

$$S(T) = 2 \sum_{q=n,p} \sum_k \ln \left[1 + \exp\left(-E_q^k/T\right)\right] + \frac{E_q^k/T}{1 + \exp\left(-E_q^k/T\right)}, \tag{10}$$

$$U(T) = E(T) - E(T=0), \tag{11}$$

where the total energy is given by

$$E(T) = \sum_{q=n,p} \sum_k \varepsilon_q^k \left[1 - \frac{\varepsilon_q^k - \lambda_q}{E_q^k} \tanh\left(\frac{E_q^k}{2T}\right)\right] - \frac{\Delta_q^2}{G}, \tag{12}$$

and $E_q^k = \sqrt{(\varepsilon_q^k - \lambda_q)^2 + \Delta_q^2}$ is the quasiparticle energy. The lengthy expression for the determinant $D(T)$ can be found in [51]. The usual T-dependent BCS equations determine the gap parameter Δ_q and the chemical potential λ_q as a function of the constant pairing strength G_q

$$N_q = \sum_k \left[1 - \frac{\varepsilon_q^k - \lambda_q}{E_q^k} \tanh\left(\frac{E_q^k}{2T}\right)\right], \tag{13}$$

$$\frac{2}{G_q} = \sum_k \frac{1}{E_q^k} \tanh\left(\frac{E_q^k}{2T}\right). \tag{14}$$

The J dependence is obtained in the usual Gaussian approximation (Eq. (5)) with the spin cut-off parameter for axially-deformed nuclei derived from the summation on the projection on the symmetry axis of the single-particle angular momentum ω_q^k

$$\sigma^2(T) = \frac{1}{2} \sum_{q=n,p} \sum_k {\omega_q^k}^2 \operatorname{sech}^2\left(\frac{E_q^k}{2T}\right). \tag{15}$$

This approach has the advantage of treating in a natural way shell, pairing, and deformation effects on all the thermodynamic quantities. The computation of the NLD by this technique corresponds to the exact result that the analytical approximation tries to reproduce, and remains by far the fastest and most reliable method for estimating NLD (despite some inherent problems related to the choice of the single-particle configuration and pairing strength). A NLD formula based on the ETFSI ground state properties (single-particle level scheme and pairing strength) has been proposed in [48]. Though it represents the first

global microscopic formula which could decently reproduce the experimental neutron resonance spacings, some large deviations, for example in the Sn region, are found (see Fig. 4). These deficiencies are cured in the new HFBCS-based model [52] which predicts all the experimental s-wave resonance spacings with an accuracy of typically a factor of about 2, which is comparable to the one obtained by the phenomenological BSFG formula (Fig. 4). The microscopic NLD formula also gives reliable extrapolation at low energies where experimental data on the cumulative number of levels is available. Furthemore, the microscopic model is renormalized on experimental (neutron resonance spacings and low-lying levels) data to account for the available experimental information. The HFBCS-based model can now be used in practical applications with a high degree of reliability. NLD's are provided in a tabular form in order to avoid the loss of precision with analytical fits.

In spite of the good aforementioned agreement between the BSFG and HFBCS-based level density predictions when experimental data are available, Fig. 5 shows that large differences may exist between them for nuclei located far from the line of nuclear stability. Important effort still has to be made to improve the microscopic description of collective (rotational and vibrational) effects, and the disappearance of these effects at increasing energies. Coherence in the pairing treatment of the ground- and excited-state properties also needs to be worked out more deeply. Global combinatorial calculations (e. g., [53]) will also increase the reliability of the NLD predictions for exotic nuclei. Experimental information, as

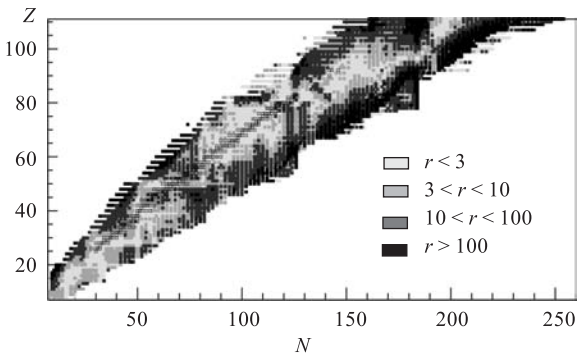

Fig. 5. Comparison between the state densities $\omega(U)$ (see Eq. (9)) at the neutron separation energy $U = S_n$ calculated by the HFBCS and BSFG models already selected in Fig. 4. The values of r displayed for all nuclides in the ranges N and $Z \geq 8$ and $Z \leq 110$ located between the proton and neutron drip lines are defined as $r = 10^{|\log(\omega_{\mathrm{HFBCS}}/\omega_{\mathrm{BSFG}})|}$. Its values are coded as indicated in the figure

provided by the primary γ-ray spectra (e. g., [54]) will strongly help in the near future to orientate microscopic models.

1.4. Optical Potential. Due to the specific requirements in astrophysics, the phenomenological potential of Woods–Saxon type has been replaced by the nucleon-nucleus optical potential [20, 55] derived from a Reid's hard core nucleon–nucleon interaction by applying the Brückner–Hartree–Fock approximation. This so-called JLM potential has recently been updated by [56] who empirically renormalized the energy dependence of the potential depth to reproduce scattering and reaction observables for spherical and quasispherical nuclei between ^{40}Ca and ^{209}Bi in a large energy range from the keV region up to 200 MeV. The resulting real (V) and imaginary (W) components of the JLMB nucleon (upper sign for neutrons and lower for protons) potential

$$V(E) = \lambda_V(E) \left[V_0(E) \pm \lambda_{V_1} \frac{\rho_n - \rho_p}{\rho_n + \rho_p} V_1(E) \right], \tag{16}$$

$$W(E) = \lambda_W(E) \left[W_0(E) \pm \lambda_{W_1} \frac{\rho_n - \rho_p}{\rho_n + \rho_p} W_1(E) \right] \tag{17}$$

are expressed as a function of the density distributions ρ, and the isoscalar (V_0) and isovector (W_0) potentials to ensure the Lane consistency, i. e., the isospin symmetry. The isoscalar normalization coefficients λ_{V,V_1} are determined mainly on elastic scattering differential cross sections and the isovector coefficients λ_{W,W_1} on quasi-elastic (p, n) scattering observables. The resulting parametrization is characterized in particular by an isovector component of the imaginary part which is about 50 % larger than the original contribution of [20]. At large neutron excesses, this enhancement reduces the imaginary component, i. e., the neutron absorption channel, and consequently the radiative neutron capture cross section. The weakness of the present BHF approaches lies in the fact that the asymmetry component of the JLMB semimicroscopic model is obtained by differentiating a symmetric nuclear BHF matter calculation with respect to the asymmetry parameter. Future BHF calculations of the asymmetric nuclear matter, such as [57], would be most useful to test this crucial effect at large neutron excesses. This semimicroscopic potential gives satisfactory results, though some improvements might be required in the low-energy description of the potential and the treatment of deformed nuclei.

Regarding the α-nucleus optical potential, the situation is less optimistic. This results from the lack of a large enough body of experimental data for sub-Coulomb cross sections combined with the difficulties to construct global and reliable α-nucleus optical potential. These theoretical problems are magnified by the fact that, at the sub-Coulomb energies of astrophysical relevance, the reaction rate predictions are highly sensitive to these potentials through the corresponding α-particle transmission coefficients. Global potentials of the Woods–Saxon type

(e. g., [58]) mainly determined on the basis of elastic scattering data at energies above the Coulomb barrier have been found to give rise to poor predictions when extrapolated at low energies, as shown by the $^{144}\mathrm{Sm}(\alpha,\gamma)^{148}\mathrm{Gd}$ experiment [59].

An attempt to develop a global α-nucleus optical potential to describe scattering and reaction cross sections in the low energy region ($E \lesssim 20$ MeV) with relevance to astrophysics has been developed in the Woods–Saxon [60] and double folding [61, 62] approaches. In the latter, the real part of the optical potential is obtained by the double-folding procedure using the M3Y nucleon–nucleon interaction [63], i. e.,

$$V_{\mathrm{df}}(\mathbf{R},E) = \iint \rho_p(r_p)\rho_T(r_T)v_{\mathrm{eff}}(E,\rho = \\ = \rho_p + \rho_T, s = |\mathbf{R} + \mathbf{r}_p - \mathbf{r}_T|)d^3r_p d^3r_T, \quad (18)$$

where $\rho_p(\mathbf{r}_p)$ and $\rho_T(\mathbf{r}_T)$ are the density distributions of the projectile and target, respectively; $\mathbf{R}$ is the separation of the centres of mass of the target and the projectile, and v_{eff} is the effective NN interaction, which depends on energy E and local densities ρ_p and ρ_T. As α is a spinless particle, only the isoscalar $v_{\mathrm{eff}}(S=0,T=0)$ component of the effective interaction is considered. The M3Y effective interaction is given

$$v_{\mathrm{eff}}(E,\rho,s) = g(E,s)f(E,\rho) \quad (19)$$

with

$$g(E,s) = 7999\frac{\exp(-4s)}{4s} - 2134\frac{\exp(-2.5s)}{2.5s} + J_{00}(E)\delta(s), \quad (20)$$

where the single nucleon exchange term J_{00} is

$$J_{00}(E) = -276(1 - 0.005E_p/A_p) \quad (21)$$

and E_p/A_p is the energy per nucleon of the projectile. The density dependence is obtained by means of

$$f(\rho) = C[1 + \alpha\,\mathrm{e}^{-\beta\rho}], \quad (22)$$

where the energy-independent parameters C, α, and β are determined by fitting the volume integral of $v_{\mathrm{eff}}(E,\rho,s)$ to the strength of the real G-matrix effective interaction obtained from Brueckner–Hartree–Fock calculations for nuclear matter of various densities ρ and at various energies [20].

As far as the imaginary part is concerned, large uncertainties on the theoretical formulation still exists. In particular, the volume or surface character of the potential is still difficult to ascertain. The imaginary part is the most of the time

described by a Woods–Saxon form with energy-independent geometry parameters. Three types of imaginary potentials were constructed by [62] from the assumption of volume or surface absorption, or from the adoption of the so-called dispersion relations that link the real and imaginary parts of the optical potential. The diffuseness and radius of these potentials have been chosen to be constant or to depend on the mass number. The energy dependence of the depth of the volume and surface terms of the imaginary potential is given by a Fermi-type function instead of the conventional Brown–Rho parametrization, and the parameters are adjusted to reproduce the experimental scattering and reaction data.

The three resulting global α-nucleus optical potentials derived by [62] are able to reproduce the bulk of the existing experimental data at low sub-Coulomb energies. However, experimental data at low energies [scattering data, α-capture or (n, α) cross sections] are scarce, particularly for masses $A > 100$, making the predictive power of the new parametrizations still uncertain. Cross sections predicted with the different potentials can differ by more than one order of magnitude at energies of relevance in astrophysics. The different potentials can be regarded as providing the uncertainty level up to which we are able today to predict globally α-induced reaction cross sections. Additional experimental data, extending over a wide mass range (especially low-energy radiative captures in the specific mass range $A \simeq 100$ and $A \simeq 200$), are of paramount importance to further constrain the determination of a reliable global α-nucleus optical potential at low energies. Much theoretical and experimental work remains to be done in this area.

1.5. γ-Ray Strength Function. The total photon transmission coefficient from a compound nucleus excited state is one of the key ingredients for statistical cross section evaluation. It strongly depends on the low-energy tail of the giant dipole resonance (GDR), which generally dominates on the $M1$ transition. The photon transmission coefficient is most frequently described in the framework of the phenomenological generalized Lorentzian model [64–66]. In this approximation,

$$T_{E1}(\varepsilon_\gamma) = \frac{8}{3}\frac{NZ}{A}\frac{e^2}{\hbar c}\frac{1+\chi}{mc^2}\ \frac{\varepsilon_\gamma^4\ \Gamma_{\mathrm{GDR}}(\varepsilon_\gamma)\varepsilon_\gamma^4}{(\varepsilon_\gamma^2 - E_{\mathrm{GDR}}^2)^2 + \Gamma_{\mathrm{GDR}}^2(\varepsilon_\gamma)\varepsilon_\gamma^2}, \tag{23}$$

where E_{GDR} and Γ_{GDR} are the energy and width of the GDR; m is the nucleon mass and $\chi \simeq 0.2$ is an exchange-force contribution to the dipole sum rule. This model is even the only one used for practical applications.

The Lorentzian GDR approach suffers, however, from shortcomings of various kinds. On the one hand, it is unable to predict the enhancement of the $E1$ strength at energies below the neutron separation energy demonstrated by nuclear resonance fluorescence experiments [68]. This departure from a Lorentzian profile may manifest itself in various ways, and especially in the form of the so-called pygmy $E1$ resonance which is observed in fp-shell nuclei, as well as in heavy

spherical nuclei near closed shells (Zr, Mo, Ba, Ce, Sn, and Pb). On the other hand, even if a Lorentzian function provides a suitable representation of the $E1$ strength, the location of its maximum and its width remains to be predicted from some underlying model for each nucleus. For astrophysical applications, these properties have often been obtained from a droplet-type of model [69]. This approach clearly lacks reliability when dealing with exotic nuclei as those involved in the r process. In view of the fact that the GDR properties and low-energy resonances may influence substantially the predictions of radiative capture cross sections, it is clearly of substantial interest to develop models of the microscopic type which are hoped to provide a reasonable reliability and predictive power for the $E1$-strength function. Attempts in this direction have been conducted within models like the thermodynamic pole approach [47], the theory of finite Fermi systems or the QRPA approximation [67]. The spherical QRPA model making use of a realistic Skyrme interaction (the Sly4 Skyrme force) has even been used

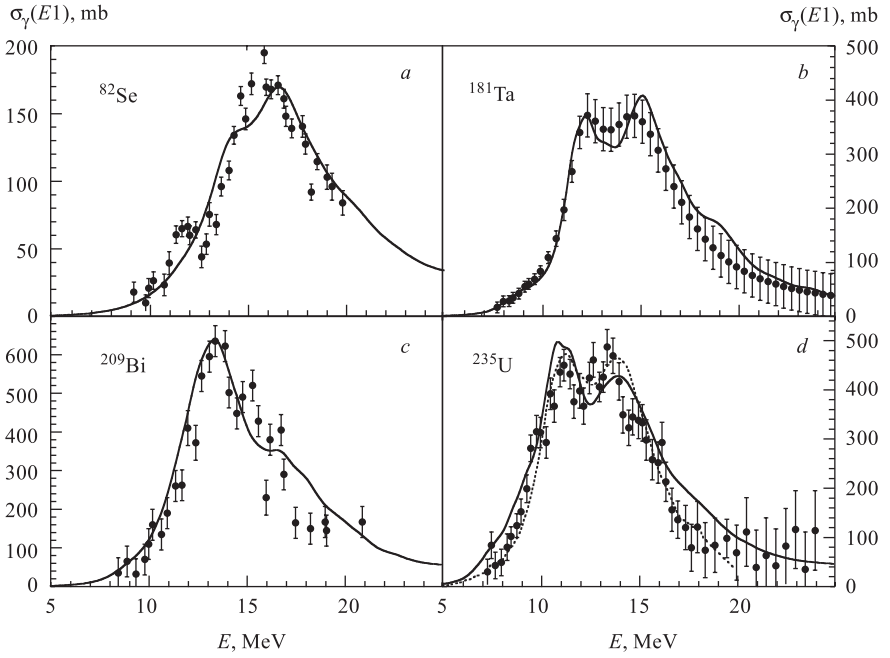

Fig. 6. Comparison of the QRPA predictions (solid line) with the experimental photoabsorption cross sections [71] (circles) for ^{82}Se (*a*), ^{181}Ta (*b*), ^{209}Bi (*c*), and ^{235}U (*d*). The QRPA peak energies were slightly renormalized to reproduce the experimental GDR energy. The dash line shown for ^{235}U corresponds to the cross section recommended by the Obninsk evaluated photonuclear library [71]

recently for *large-scale* derivations of the $E1$-strength function [70]. This global calculation predicts the location of the GDR energy in close agreement with experimental data, the r. m. s. deviation of the predictions from measurements for 84 nuclides amounting to about 300 keV only. The final $E1$-strength functions are obtained by folding the QRPA strengths with a Lorentzian function to take the deformation effects and the damping of the collective motion into account. The QRPA $E1$-strength functions reproduce satisfactorily the photoabsorption [47,71], as well as the average resonance capture data at low energies [65]. We illustrate in Fig. 6 how the QRPA calculation reproduces the photoabsorption cross sections of four (spherical and deformed) nuclei in the whole GDR region [71]. In particular, the GDR energy and width, as well as the double peak structure observed experimentally are rather well reproduced by the QRPA model.

The aforementioned QRPA calculations have been performed for all the $8 \leq Z \leq 110$ nuclei lying between the two drip lines. In the neutron-deficient region, as well as along the valley of β stability, the QRPA distributions are very close to a Lorentzian profile. Significant departures from a Lorentzian are found for neutron-rich nuclei. In particular, QRPA calculations show that the neutron excess affects the spreading of the isovector dipole strength, as well as the centroid of the strength function. The energy shift is found to be larger than predicted by the usual $A^{-1/6}$ or $A^{-1/3}$ dependence given by the phenomenological liquid drop approximations [69]. In addition, some extra strength is predicted to be located at sub-GDR energies, and to increase with the neutron excess. The more exotic the nucleus, the stronger this low-energy component. This is illustrated in Fig. 7 for the $E1$-strength function in the Sn isotopic chain. Among the 8 distributions shown in Fig. 7, only the $A = 150$ one corresponds to a deformed configuration responsible for the double peak structure. For the $A \geq 140$ neutron-rich isotopes, an important part of the strength is concentrated at low energies ($E \lesssim 5{-}7$ MeV). Phenomenological models are unable to predict such low energy components, whatever their collectivity is. In particular for ^{150}Sn, all phenomenological systematics (as used for cross section calculation) predict a γ-ray strength peaked around 15 MeV with a full width at half maximum of about 4.5 MeV [47] which is obviously very different from the microscopic estimate (Fig. 7). The above-described fea-

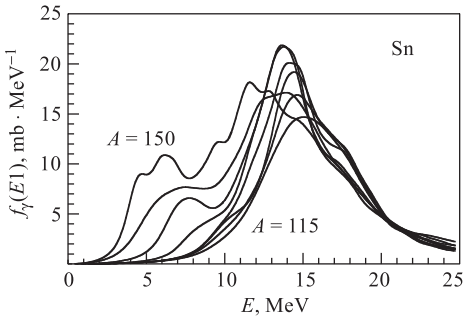

Fig. 7. $E1$-strength function for the Sn isotopic chain predicted by the QRPA with the SLy4 Skyrme force. Only isotopes ranging between $A = 115$ and $A = 150$ by steps of $\Delta A = 5$ are displayed

ture of the QRPA $E1$-strength function for nuclei with a large neutron excess is found to be qualitatively independent of the adopted effective interaction [70]. Even if the low-lying strength represents only about a few percent of the total $E1$ strength, it can produce an increase by up to an order of magnitude of the radiative capture rate by some exotic neutron-rich nuclei and influence the production of neutron-rich nuclei by the r process [66, 70]. Future HFB-QRPA calculations including deformation effects will hopefully increase the reliability of the present predictions. The microscopic treatment of the spreading width is of great importance [72].

2. TOWARDS A SELF-CONSISTENT PREDICTION OF WEAK INTERACTION RATES

Weak interaction rates are important ingredients in the modeling of practically all stellar processes — the hydrostatic burning of massive stars, late (pre-supernova) stage of their evolution, production of heavy elements in stellar nucleosynthesis via s, p, r, rp processes. We will limit ourselves here to the problem of large-scale predictions of the weak interaction rates for the modeling of the heavy elements nucleosynthesis via the r process. In Secs. 2, 4, we will give a detailed overview of the existing approaches to the β^--decay and $\nu_e(\bar{\nu}_e)$-capture rates, discuss the main unsolved problems, and demonstrate the performance of the models comparing their results with available experimental data. A discussion of the shell-model results concerning the electron capture and β^- decay, as well as the inelastic $\nu_e(\bar{\nu}_e)$ scattering on the presupernova phase of massive stars can be found in the review [73].

The canonical model which assumes that the r process is governed by the multiple neutrons captures and successive β^- decays at stellar environments [74] gives only a general picture of the r process. According to currently favored scenario, the plausible r-process site might be related to the so-called neutrino-driven wind [75–77] blown out the surface of hot proto-neutron star after core collapse of a type II supernova. The neutrino-heated supernova ejecta appear to be a promising site for nucleosynthesis of heavy elements, in spite of the numerous modeling difficulties that still remain to be overcome. The shock-heated (dissociated) helium shells in type II supernovae [78], and neutron star mergers [79] are actively studied as alternative sites. In all these models it is assumed that the ejected material is exposed to extreme fluxes of the neutrinos of all flavors.

In addition to numerous problems in the quest of the astrophysical site for the r process, nuclear physics uncertainties are still high. To perform a network calculation of the elemental production in the r process, the knowledge of the properties of thousands of (mostly unknown) neutron-rich nuclei is required (see

Introduction). Those include the characteristics of strong, electromagnetic and weak interaction processes. In particular, β^- decays play a key role since they are the major mechanism for driving the material to heavier elements and for setting the r-process time scale. In the case where the r process takes place in a neutrino-rich environment, charged-current electron neutrino capture could amplify the effect of β^- decays. It could also change the r-abundance distribution by subsequent ν-induced neutron spallation [80]. Hence, it is of great importance to make reliable predictions of nuclear weak interaction rates for very neutron-rich nuclei. Parametrized nuclear models exclusively fitted to experimental data close to the β-stability line are not expected to give rise to reliable extrapolations at extreme isospin values. As already emphasized in Introduction, the r-process nucleosynthesis calculations depend both on nuclear masses and β rates, so it is crucial that the predictions of the β-decay and ν_e-capture rates are based on the same ground state description as the one used to estimate the reaction rates, and in particular the nuclear masses.

2.1. β-Strength Function and β-Decay Rates. The elementary particles weak interaction rates are adequately calculated within the Standard model of electroweak interaction. The smallness of the weak interaction couplings between the quarks and leptons justifies the treatment of the weak processes involving atomic nuclei (semileptonic processes) in the lowest-order approximation. For this reason, the treatment of weak nuclear processes rates reduces to a nuclear structure problem. It is convenient to introduce the β-strength function, i. e., the spectral distribution of the β-decay transition matrix elements.

The total half-life of the β^--decay process $A_Z(J^\pi) \to A_{Z+1}(J'^{\pi'}) + e^- + \bar{\nu}_e$ in the β-strength function formalism is calculated as

$$1/T_{1/2} = D^{-1}(G_A/G_V)^2 \int_0^{Q_\beta} d\omega f_0(Z,\omega) \sum_n \langle \kappa_J \rangle S_n(\omega,\gamma), \qquad (24)$$

where ω stands for the β-decay transition energy; $Q_{\beta^-} = \Delta B + 0.782$ MeV is the β-decay energy window; B is the difference of total nuclear binding energies of the parent and daughter nuclei, and γ is the width of individual excitation which may be introduced to simplify the numerical calculations. Notice, though the excitation energies in the daughter nuclei are used for the experimental decay schemes, the adequate variables within the RPA-type approaches are the β-decay transition energy ω relative to the parent nucleus ground state and the electron energy. The total half-life depends directly on the Q_β value only for the case of the g. s.-to-g. s. transition, otherwise it depends on the energies of the strongest transitions with the lowest degree of forbiddeness. The sum contains the Gamow–Teller (GT) term with $J = 1$ and the first-forbidden (FF) terms with $J = 0, 1, 2$. For the GT and nonunique FF decays $\langle \kappa_{J=0,1} \rangle = 1$, and for the unique FF decays, $\langle \kappa_{J=2} \rangle = f_1/f_0$, with the Fermi integral f_1 calculated as in [81]. The integrated

lepton $(e^-, \bar{\nu}_e)$ phase-space volume for allowed transitions

$$f_0 = \int_{m_e c^2}^{W_{\max}} F(Z,W) pW (W_{\max} - W)^2 dW \tag{25}$$

incorporates the Coulomb and finite-size corrections [82]. The nuclear structure effects are incorporated in the corresponding β-decay strength functions $S_n(\omega, \gamma)$.

In early works, the strength functions for large-scale astrophysical applications have mostly been treated empirically. The first large-scale evaluation of the β^--decay rates for the heavy nuclei involved in the r process was made by [74] making use of an energy independent β-strength function and the allowed transition approximation. In later works, statistical arguments were used to justify a smooth energy dependence of the β-strength function taken to be proportional to the level density of low-lying states in the daughter nucleus [83]. However, the numerous measurements including the recent RIB experiments have shown that the β-strength function presents a typical resonance structure which is quite pronounced in spherical nuclei and is more spread out in deformed ones. Such a nonstatistical behaviour originates from the basic selection rules and modification of the β-strength function due to the effects of the pairing and effective NN interactions (for review see [84]). This gives natural grounds for microscopic approaches to nuclear weak processes.

2.2. Global Models for β-Decay Calculations. Turning to the global, unified approaches relying on the microscopic nuclear structure models was a principal step forward in the analysis of stellar nucleosynthesis. In general, the models for global calculations of the β-decay rates created in the last decades can be divided as the parametric «gross theory»-like models, microscopic models with empirical mean-field potentials, and self-consistent mean-field models.

The first parametric model for β rates which attempted to combine the single-particle and statistical arguments in a phenomenological way is the so-called «gross-theory» [85]. Within this framework, the β-strength function of extreme single-particle model is folded over the Fermi gas level density corrected for the pairing and shell effects. On top of that, the smooth contributions of the tail of the giant GT, spin-dipole and (Δ, N^{-1}) resonances are also included in a purely parametric way. A Gaussian or Lorentz shape is adopted for these resonances with an energy, position, strength, and width fitted to the available experimental data, the sum rules, and finally the measured half-lives. Recent improvements in the so-called GT2 and semi-gross theory [86, 87] use an updated mass formula and give a better account for the shell and pairing effects. The limitations of the method are intrinsically related to its «micro-statistical» origin. As for the specific nuclear structure concept of the model, it has a serious deficiency of neglecting the coherent effects due to the effective NN interaction. The single-particle model eventually overestimate the β-decay energies and strengths of the

high-energy β transitions. Thus the «gross-theory»-like parametrizations tend to underestimate the β-decay half-lives. Up to now, the later versions of the «gross theory» [86, 87] have been used for the practical applications because of their accurate reproduction of the experimental data and available extrapolation to unknown nuclei.

The hybrid approaches based on a mixture of the microscopic and statistical inputs offer successful parametrizations in the regions relatively close to the β-stability line. However, the reliability of their extrapolation far off stability can be questioned. From general considerations, the more consistent the model, the less parameters are involved and the sounder the extrapolation away from the stability line. Of course, it is not just the microscopic origin of the model that can solve the problem. For a reliable global prediction of all weak rates (including for experimentally unreachable nuclei), a sufficiently extended nuclear structure framework needs to be developed.

• First, as already has been stressed, the β-strength function calculations should be based on the self-consistent ground state description, namely on the same, as used to calculate the nuclear masses. This is especially important for the modeling of the isotopic composition of the elements produced in the r process which depends both on nuclear masses and β rates.

• Second, to use the key advantage of the self-consistent approach, the model should employ a universal (A-independent) spin-isospin NN interaction, as well as universal (and energy independent) quenching factors. To allow that, the model should operate with unrestricted single-particle basis. This feature of the model is of prime importance for large-scale calculations.

• Third, it is crucial for the β-decay model to predict the correct amount of both the integral strength, and its spectral distribution within the Q_β window. In fact, the constraints are even more strict, since one needs to describe properly both the low energy β^--strength distribution and the correct position and strengths of the GT and spin-multipole resonances in the continuum for calculating the (ν_e, e^-) rates (see Sec. 2.6).

While the independent particle model gives too much β strength in the Q_β window, the use of pure repulsive contact interaction in RPA calculations systematically underestimates the β^- strength (which for most of the nuclei normally constitutes only a few percent of the Ikeda sum-rule!) resulting in too long half-lives [95]. The reasonable effective spin-isospin NN interactions in the particle-hole (ph) and particle-particle (pp) channels should provide an appropriate balance between the repulsive and attractive components, as well as between its contact and finite-range parts.

The possibility for microscopic large-scale predictions of the β-decay half-lives has been already demonstrated in [96] where the authors developed a schematic three-level (RPA-like) model in the framework of the finite Fermi system theory (FFS) [97]. In this simplified model, an advantage however was taken

of the universal Landau–Migdal effective NN interaction with the single parameter g' being constrained from $SU(4)$-symmetry arguments. In the recent years, two fully microscopic approaches have been used for the large-scale calculation of weak rates for astrophysical applications — the shell model and the quasiparticle random-phase approximation (QRPA). The advantage of the shell-model is the possibility of taking into account the detailed structure of the β-strength functions. On the other hand, the QRPA models have basically no limitations in calculating heavy and even superheavy nuclei.

Up to now, the shell-model calculations have been performed for electron capture and β-decay rates [73] for nuclei of importance in the modeling of the pre-supernova stage of massive stars, as well as for specific neutron-rich nuclei along the isotones at $N = 50, 82$ [88] and also $N = 126$ [89]. The «no-core» shell-model calculations using the effective interactions and multi-$\hbar\Omega$ model space are feasible for the GT decay of light nuclei [90]. For heavier nuclei, the determination of the GT strength distribution requires such a large shell-model diagonalization (accounting for all correlations among the valence nucleons in a major oscillator shell) that a truncation of the basis complemented by a renormalization of the GT β-decay operator is inevitable. Since the FF decays involve different oscillator shells, a multi-$\hbar\Omega$ treatment is needed in this case. A restricted «valence-core» calculation of the forbidden decays in the tin and lead region was performed by [91]. The shell model with continuum has also been applied to the β decay of light nuclei [92]. The recently developed density matrix renormalization group method [93] could be helpful for large-scale shell-model calculations. The generic problem related to the self-consistency of the multi-$\hbar\Omega$ shell-model calculations has been discussed in [94].

As the QRPA approach is free of the above-mentioned limitations, it is probably the most suited for dealing with heavy nuclei, and for predicting their half-lives in particular. Several types of large-scale QRPA-type calculations of weak rates can be found in the literature. The first QRPA-type models for the $\beta^{\pm}$-decay half-lives rely on schematic (separable) effective NN interactions and (empirical) deformed single-particle potentials [98]. This was an important step which has made the large-scale calculations of the weak rates feasible even for limited computer powers at that time. The RPA model of the allowed β decay by [99] is based on the macroscopic-microscopic finite-range droplet mass model (FRDM) [26]. It has been used later for an extensive calculations of β-decay observables. However, a closer confrontation of the β-decay characteristics with recent experimental data on short-lived nuclei [100] reflects the generic deficiencies of the BCS + RPA-type models [98, 99]. The first one concerns the calculation of the half-lives in terms of the excitation energy relative to the daughter nucleus ground state. Clearly, the latter cannot be properly defined for empirical mean-field potentials, as the total binding energies of the parent and daughter nuclei in Eq. (24) should be calculated self-consistently.

The second one is the neglecting of the isosinglet effective NN interaction (proton-neutron $T = 0$ pairing or pp interaction) which should normally be presented in the dynamic charge-exchange QRPA equations [97, 106, 109] alongside with the ph effective interaction. (Note, the isotriplet $T = 1$ pairing between like particles has already been incorporated at the BCS level.) Omitting this specific NN interaction channel leads to spurious amplification of the odd-even effects the total β-decay half-lives. In contrary, with the pp interaction in effect, the scale of the experimental odd–even staggering of the half-lives can be correctly reproduced. The reason is that the $T = 0$ pairing increases drastically the β^+-decay half-lives [101, 102] and reduces significantly the β^--decay half-lives due to a small (few percent) decrease of the giant GT resonance matrix element which correspondingly causes an increase of the GT strength in the Q_β window [103].

Recently, the FRDM-based model has been extended to include the contribution of the FF decays. The resulting FRDM-hybrid model by [104] treats the GT transitions within the RPA; and the FF transitions, within the statistical «gross theory» framework. Since this inconsistent procedure brings macroscopic corrections to the original «microscopic» BCS + RPA model [98], it is hard to interpret the results obtained.

In the analogous model by [105] based on the deformed Nilsson + BCS formalism, the complete QRPA equations are solved using the restricted single-particle basis and separable NN interactions both in the ph and pp channels. Since the universal parametrization of these interactions in a wide mass region is problematic, a direct fitting to the experimental half-lives is performed (separately for each isotopic chain). An important extension of the model [107] includes the contribution of the configurations more complex than $1p1h$. Also the unique FF transitions are included in a microscopic way in [108] (this simplest forbidden decay channel is important in special cases only).

One has to mention that much more extended version of the approach with separable NN interaction is given by the well-known quasiparticle-phonon model (QPM) [109] with the complex configurations taken into account. It offers a possibility for a systematic study of the impact of the two- and three-phonon configurations on the weak interaction rates. An early version of the model has been used to calculate the β^+-decay strength functions of selected nuclei in [110]. The approach has been extended to employ the finite rank separable approximation for the Skyrme-type interaction with a possibility of structure calculations in large ph spaces [111]. So far, the full version of the QPM has not been applied to large-scale calculations of the weak rates.

2.3. Towards the Self-Consistent β-Decay Model. The ultimate model of the β-decay properties for astrophysical applications should be self-consistent. The ingredients of the approach are the self-consistent mean-field potential (for the ground-state properties) and the universal effective NN interaction (for de-

scription of the excited states), the both being originated from the unique nuclear energy-density functional. The concept is inspired by the energy-density functional theory based on a general property of the systems of interacting electrons, known as the Hohenberg–Kohn theorem [40]. For nuclear many-body system, the phenomenological density functional can be constructed in the local density approximation (see, i. e., [39] and Refs. therein) which, in principle, gives a possibility of describing *ab initio* the properties of nuclear ground and excited states. A substantial amount of work in this direction which has been done in the last decades is well reviewed in the literature.

The first self-consistent (HFBCS + CQRPA) model for the β-decay half-lives has been developed in [113] in the framework of the self-consistent finite Fermi system theory (SFFS) [114]. Below we briefly overview the basics of the HFBCS + CQRPA approach to the β-decay strength functions.

The ground state properties are calculated from the self-consistent mean field which is the first functional derivative of the interaction energy with respect to the normal density, while the pairing potential is obtained as the functional derivative of the pairing energy with respect to the anomalous nucleon density. The total interaction energy of superfluid nucleus, $E_{\rm int}[\rho,\nu] = \int d\mathbf{r}\, \varepsilon_{\rm int}(\mathbf{r};[\rho,\nu])$, is a functional of two densities: the normal, $\rho(\mathbf{r})$, and the anomalous, $\nu(\mathbf{r})$. Self-consistent calculation with such a functional looks like the standard variational HFB procedure in which the single-particle Hamiltonian takes the form

$$\mathcal{H} = \begin{pmatrix} h-\mu & \Delta \\ -\Delta^* & \mu - h \end{pmatrix}, \tag{26}$$

where

$$h = \frac{p^2}{2m} + \frac{\delta E_{\rm int}[\rho,\nu]}{\delta\rho}, \quad \Delta = -\frac{\delta E_{\rm int}[\rho,\nu]}{\delta\nu}. \tag{27}$$

These equations were solved iteratively. Note that h contains the free kinetic energy operator (the quasiparticle effective mass m^* being equal to the bare nucleon mass m). The interaction energy density is represented as

$$\varepsilon_{\rm int} = \varepsilon_{\rm main} + \varepsilon_{\rm coul} + \varepsilon_{\rm sl} + \varepsilon_{\rm pair}, \tag{28}$$

where $\varepsilon_{\rm main}$ contains the volume isoscalar and isovector contributions and also the surface isoscalar and isovector interaction energies generated by the density-dependent finite-range forces. The Coulomb interaction energy density $\varepsilon_{\rm coul}$ takes the usual form and includes the exchange part in the Slater approximation, while the spin-orbit term $\varepsilon_{\rm sl}$ in (4) comes from spin-orbit $\propto (\kappa + \kappa'\boldsymbol{\tau}_1\boldsymbol{\tau}_2)[\boldsymbol{\nabla}_1\delta(\mathbf{r}_1-\mathbf{r}_2)\times(\mathbf{p}_1-\mathbf{p}_2)](\boldsymbol{\sigma}_1+\boldsymbol{\sigma}_2)$ and velocity and spin-dependent $\propto (g_1 + g_1'\boldsymbol{\tau}_1\boldsymbol{\tau}_2)(\boldsymbol{\sigma}_1\boldsymbol{\sigma}_2)(\mathbf{p}_1\mathbf{p}_2)$ interactions (for details see [39]). The last term

in (4) is the pairing energy density $\varepsilon_{\rm pair} = 1/2\nu F^{\xi}\nu$, where ν is the anomalous nucleon density and F^{ξ} is an effective force in the particle–particle channel chosen in the density-dependent form as

$$F^{\xi}(\mathbf{r}_{12}) = -4N_0^{-1} f^{\xi}(x)\delta(\mathbf{r}_{12}), \tag{29}$$

where $N_0 = 150$ MeV fm^3 is the inverse half-density of states at the Fermi surface in equilibrium nuclear matter. The $f^{\xi}(x)$ is a dimensionless strength treated in the local density approximation as a (local) functional of the isoscalar density $x = (\rho_p + \rho_n)/2\rho_0$, where the $\rho_{p,(n)}$ are the proton (neutron) densities. This is expressed in a Skyrme-like form [39]

$$f^{\xi}(x) = f^{\xi}_{\rm ex} + h^{\xi}x^q(\mathbf{r}), \tag{30}$$

where $f^{\xi}_{\rm ex}$ is negative (attractive in the pp channel); $h^{\xi}x^q(\mathbf{r})$ is positive with $q = 2/3$ (a repulsive short-range part), the gradient term is omitted. The superscript ξ refers to the energy cut-off parameter. It defines the number of single-particle levels taken into account when evaluating the anomalous Green functions and, correspondingly, when solving the equations for the pairing fields $\Delta(\mathbf{r})$ and chemical potentials μ, as well as the QRPA equations for the excited states. In the case of the density dependent pairing, a local cut-off treatment of the pairing energy density [39] helps one to avoid the problem of the choice of the cut-off energy. An efficient pairing regularization procedure has been suggested recently in [135]. In the case when density-dependence is omitted, pairing is being treated in a diagonal approximation on the basis corresponding to the $\varepsilon_{\text{cut-off}} = 15$ MeV. Then the pairing strength parameter $f^{\xi} = 0.33{-}0.40$ is chosen to reproduce the empirical matrix elements of the pairing potential Δ^{τ}.

The calculations of the ground state properties are performed with the DF3 density functional [39] and the recently derived options of the Skyrme force SkSC17 [121] and MSk7 [30]. An additional self-consistency condition [130] is used to remove a spurious isospin mixing for Fermi transitions. The excited states are treated within the CQRPA-like framework of the SFFS with exact treatment of the ph continuum, density-dependent pairing, and finite-range effective NN interactions in both the ph and pp channels [113, 121, 125, 126].

The CQRPA equations for the finite Fermi system with pairing correlations [114], involve the ph, pp, and hole-hole (hh) blocks. Assuming that the effective NN interaction is nonretarded, these equations can be written in terms of the density matrix variations $\hat{\rho}_i$ in the external field $\hat{V}^0$

$$\hat{V}_i = \hat{e}_{qi}\hat{V}^0_i + \sum_k ((\hat{F}_{ik}\hat{\rho}_{ik})). \tag{31}$$

The density matrices are related to the effective fields by

$$\hat{\rho}_i = \sum_k ((\hat{A}_{ik}\hat{V}_k)), \tag{32}$$

and to a linear response theory by

$$\hat{\rho}_i = \hat{\rho}_i^0 + \sum_k ((\hat{A}_{ik}\hat{F}_{ik}\hat{\rho}_k)). \tag{33}$$

Here the 3-by-3 matrix formalism of [115] is used; $\rho = \int d\varepsilon/(2\pi i)\hat{R}_i(\mathbf{r},\mathbf{r};\varepsilon,\omega)$, $\hat{R}_j = (\delta G, \delta F^{1,2}, \delta G^h)$, $(j = 0, 1, 2, h)$ being the variations of the normal, anomalous and hole Green functions in the external fields $\hat{V}_i^0$. (Each pair of external brackets indicates the integration on the spatial coordinates and a summation on the total spins.)

The effective field supermatrix $\hat{V}_i$ consists of the ph vector $\hat{V}$ (a variation of the nonsingular term of the mass operator Σ in the external field $\hat{V}_0$), as well as of the pp and hh vectors $\hat{d}^{(1)}$, $\hat{d}^{(2)}$ (variations of the gaps $\Delta^{(1)}, \Delta^{(2)}$). The universal medium renormalization of the external fields of a different symmetry (beyond the QRPA-type correlations) is taken into account via the quasiparticle local charge operators $\hat{e}_{qi} = e_q[V_0^{JLS}]$. The so-called «quenching factor», $Q = e_{qs}[\sigma\tau]^2 = (g_A/G_A)^2$, is usually introduced in order to suppress the spin-isospin fields in the nuclear medium. The smaller Q, the less strength contained in the low-energy part ($\omega < \varepsilon_F$) of the spin-isospin response, and therefore the longer the β-decay half-lives.

In Eqs. (31)–(33), the effective NN interaction $\hat{F}$ which consists of the ph component F^ω coming from the normal part of the density functional (DF) and of the pp and hh components F^ξ is connected to pairing energy density. For the β-decay properties, the most important contribution comes from the spin-isospin effective NN interaction (the velocity-dependent terms are not included to $\hat{F}$). In the fully self-consistent approach it should be determined as the second functional derivative of the interaction energy with respect to the normal and pairing densities. The spin-dependent (time-odd) component of the DF responsible for spin-polarization properties and its scalar (time-even) part which characterizes the ground state properties are interconnected through the density dependence of the interaction. Although most of the parameters of the spin-isospin part are independent of the others, they are constrained by the values of the parameters defining the scalar part of the energy-density functional [39]. This results in some restrictions in applications of the fully self-consistent approach. The spin-isospin parameter g' derived from the available Skyrme forces in Landau limit turns out to be much lower than its empirical value [121, 127]. The alternative spin-dependent energy-density functional has not been developed yet for spin-unsaturated nuclei [39, 128].

A strategy for the large-scale calculations is found in the fact that the ground state properties are rather insensitive to the spin and spin-isospin-dependent components of the DF (except for the spin-orbit term). In a first approximation, the scalar and spin-isospin components of the energy-density functional can be decoupled and the effective NN interactions in the spin-isospin channels may be defined not as the second variance of the DF, but introduced independently [113]. This assumption spoils the formalism consistency, but can be shown to have an insignificant impact on the ground state properties. On the other hand, it has the advantage of enabling the use, in the QRPA-part of the calculation, of the well-founded spin-isospin effective NN interaction of the FFS theory [114] which is assumed to be A-independent. In the case of the DF + CQRPA approach, the Landau–Migdal constant is renormalized with respect to one derived from the Skyrme force parameters, and turns out to be very close to the empirical value, thereby ensuring a reliable description of the GT strength function in the whole energy scale.

The spin-isospin effective NN interaction in the particle-hole (ph) channel written in the transferred momenta ($\mathbf{k}$) space is

$$F^{\omega}_{\sigma\tau} = 4N_0^{-1}\left[g'_0\boldsymbol{\sigma}_1\boldsymbol{\sigma}_2 + g_\pi e^2_{q\pi}\frac{(\boldsymbol{\sigma}_1\mathbf{k})(\boldsymbol{\sigma}_2\mathbf{k})}{k^2+m_\pi^2+P_\Delta(k^2)} + \right.$$
$$\left. + g_\varrho e^2_{q\rho}\frac{[\boldsymbol{\sigma}_1\mathbf{k}][\boldsymbol{\sigma}_2\mathbf{k}]}{k^2+m_\varrho^2}\right]\tau_1\tau_2. \quad (34)$$

Here, $N_0 = 150$ MeV fm^3 is the normalization factor; $g_\pi = -2\pi/N_0\ (f_\pi^2/m_\pi^2)$, $g_\varrho = -2\pi/N_0\ (f_\varrho^2/m_\varrho^2)$, where $m_\pi(m_\varrho)$ and $f_\pi(f_\varrho)$ are the bare pion (ϱ-meson) mass and the $\pi NN(\varrho NN)$ coupling constants, respectively. The pion irreducible polarization operator in the nuclear medium $P_\Delta(k^2)$ takes care of the virtual Δ isobar–nucleon hole excitations. The contact part of the effective spin-isospin interaction Eq. (14) is governed by the Landau–Migdal constant g'_0. The operator $e^2_{q\pi} = Q = e_q[\sigma\tau]^2$ is assumed to describe the quenching of the pion-nucleon vertex [114]. The operator $e^2_{q\varrho}$ is defined from the condition that the ϱNN coupling strength is $g_\varrho = 0.4g_\varrho^{\rm bare}$ due to the short-range NN correlations.

The one-π and one-ρ exchange terms modified by the nuclear medium are important in describing the magnetic properties of nuclei and the nuclear spin-isospin responses. The competition between the one-pion attraction $g_\pi Q < 0$ and spin-isospin repulsion $g'_0 > 0$, determines a degree of «softness» of the pionic modes in nuclei that influences directly the β-decay half-lives. So far, two basic sets of FFS parameters have been found to describe satisfactory the spin-isospin nuclear properties: (A) $Q = 0.81$, $g\prime = 0.9{-}1.0$ derived from the magnetic moments [114], which allows for a moderately soft π-modes [116]; (B) $Q = 0.64$, $g\prime = 1.0{-}1.1$ derived from observed GT and $M1$ strength distributions [117,130]. A strong quenching excludes the existence of soft π-modes. The recent analysis of (p,n) reaction spectra at $E_p = 295$ MeV [119] and excitation energies up to

$E_x < 50$ MeV gives some evidences for $Q = 0.93 \pm 0.05$, i. e., of a lower quenching than previously expected from the old (p, n) data at $E_x < 30$ MeV [118]. The experimental uncertainties remain still large, and both sets should be applied in the calculations of the β-decay half-lives.

In a general case, the spin-isopsin ($T = 0$) effective NN interaction in the pp channel can be chosen in a form similar to the one for $T = 1$ pairing:

$$F^{\xi}_{\sigma\tau}(\mathbf{r}_{12}) = -4N_0^{-1} G'_{\xi}(x)\delta(\mathbf{r}_{12}) \quad (J^{\pi} = 0^-, 1^+, \dots). \tag{35}$$

The $G^{\xi}(x)$ is a dimensionless strength depending on the isoscalar density $x = (\rho_p + \rho_n)/2\rho_0$, where the $\rho_{p,(n)}$ are the proton (neutron) densities. This is expressed in a Skyrme-like form $G^{\xi}(x) = g'_{\xi} + h^{\xi} x^q(\mathbf{r})$, where g'_{ξ} is negative (attractive in the pp channel), $h^{\xi} x^q(\mathbf{r})$ is positive with $q = 2/3$ (a repulsive short-range part) [39]. The superscript ξ refers to the energy cut-off parameter. It defines the number of single-particle levels taken into account when evaluating the anomalous Green functions and, correspondingly, when solving the equations for the pairing fields $\Delta(\mathbf{r})$ and chemical potentials μ, as well as the QRPA equations for the excited states. In the case of the density dependent pairing, a local cut-off treatment of the pairing energy density [39] helps to avoid the problem of the choice of the cut-off energy. An increase of g'_{ξ} leads to shorter β^--decay half-lives and softer (p, n) spectra (longer β^+-decay half-lives and harder (n, p) spectra) [101–103]. This allows us to select $g'_{\xi} = 0.3 \div 0.5$ for the density-independent pairing (with $E_{\text{cut-off}} = 15$ MeV) from the recent (n, p) reaction data in the Fe-Co-Ni region (see [147] and Refs. therein).

The QRPA-propagator supermatrix $\hat{A}$ is obtained by integrating various pair products of the Green functions over the energy variable ε. To avoid the ph-basis truncation (inevitable in the λ representation), Eqs. (31) can be solved in the mixed (r, λ)-approximation. The idea of the method is physically transparent: the nuclear pairing is important within the «valence λ-space» only. It is defined as $\mu^{\tau} - \xi < \varepsilon < \mu^{\tau} + \xi$, where μ^{τ} are the neutron and proton chemical potentials. The corresponding part of the propagator L is constructed in the λ space and transformed to the r space. For the states far from the Fermi surface the propagator matrix degenerates into a single ph propagator $\tilde{A}$ of the system with no pairing. It is calculated via the Green functions constructed in the r space which allows the exact inclusion of the ph continuum. Thus, the full propagator reads

$$A(\mathbf{r}, \mathbf{r}'; \omega) = \tilde{A}(\mathbf{r}, \mathbf{r}'; \omega) + \sum [L_{pn}(\omega) - \\ - \tilde{A}_{pn}(\omega)] \varphi^*_n(\mathbf{r}_1)\varphi_p(\mathbf{r}_1)\varphi_n(\mathbf{r}_2)\varphi^*_p(\mathbf{r}_2), \tag{36}$$

where φ_{τ} are the single-particle wave functions, and $\tilde{A}_{pn}$ term, i. e., the part of the propagator A corrected for the pairing contribution is subtracted to avoid a

double counting. The (r, λ) approximation was firstly developed for the non-charge-exchange case in [115], and then extended for the charge-exchange excitations in [103] (for the complete formulae including the important case of the odd-A nuclei see [112]).

For the decay to the states with $Q_\beta - \omega > S_n$, it is convenient to use the partial β-strength functions

$$S_\beta^{JLS}(\omega,\gamma) = \frac{(2J+1)}{4\pi}(e_q^{JLS})^2 \int \hat{V}_0^{JLS}(r)\hat{\rho}^{JLS}(r;\omega,\gamma)r^2 dr, \qquad (37)$$

here S_n is the neutron separation energy in the daughter nucleus; $\hat{\rho} = N\,\mathrm{Im}\,(\hat{A}\hat{V})$ are the density matrices of Eq. (32) (the explicit formulae involving the ph, pp, and hh component can be found in [112]). The transition density is normalized on the matrix element of the transition $|0\rangle \to |s\rangle$

$$\mid M_{\mathrm{os}} \mid^2 = (2J+1) \mid e_q^{JLS} V_0^{JLS}(r)\rho_{\mathrm{tr}}^{JLS}(r,\omega_s) \mid^2 = \int\limits_{\Delta\omega_s} S_\beta^{JLS}(\omega,\gamma)d\omega. \qquad (38)$$

Here, the energy interval $\Delta\omega_s = \Gamma_{\mathrm{esc}} + 4\gamma$ includes the state $|s\rangle$ located within the β-decay window, Γ_{esc} being the corresponding escape width; and $\Gamma^{\downarrow} = 4\gamma$ is the artificial width of the individual excitation which may be introduced in order to simplify numerical integration. After the strength function $S_\beta^{JLS}(\omega)$ has been found, the total half-lives can be evaluated from Eq. (24). One has to stress that no direct fitting to the experimental half-lives is performed.

Due to the computational limitations, only the ETFSI + CQRPA version of the self-consistent model elaborated in [120] has been applied so far to the coherent large-scale predictions of nuclear masses, β^--decay rates, and ν_e-capture rates in [121, 122], as well as $\bar{\nu}_e$-capture rates in [123]. The self-consistent treatment within the ETFSI model of the ground state properties and consideration of the pp effective interaction resulted in a more realistic evaluation of odd–even effects in the total half-lives [113, 120, 121] compared to the FRDM Tables [99]. As it has been long argued, the relative contribution of the GT and FF β decays may vary in the vicinity of the $Z \geq 50$ nuclei near $N = 82$ and for the nuclei near $N = 126$ [121, 129]. However, so far no microscopic large-scale calculations of the half-lives have been performed beyond the allowed β-decay approximation.

After the first competitive HFBCS mass table has appeared [30], the corresponding HFBCS + CQRPA model for the weak rates has been suggested in [125, 126]. It is based on the ground state description given by the Skyrme-MSk7 force [30] or alternatively DF3 density functional [39, 113]. The important feature of the method is that contribution of both the GT and FF transitions is considered microscopically. The allowed GT and first-forbidden decays from the parent nucleus ground state $|i\rangle$ to the final states $|f\rangle$ of the daughter nucleus depend on seven β moments related to the nuclear matrix elements of the following

operators

$$\begin{gathered}\boldsymbol{\sigma},\\ \gamma_5, [\boldsymbol{\sigma}\mathbf{r}]^{(0)},\\ \alpha, \mathbf{r}, [\boldsymbol{\sigma}\mathbf{r}]^{(1)},\\ [\boldsymbol{\sigma}\mathbf{r}]^{(2)},\end{gathered}$$

where $\boldsymbol{\sigma}$ are the Pauli spin matrices, and the rank of the tensor operators $[\boldsymbol{\sigma}\mathbf{r}]^{(J)}$ is defined by the momentum $|J_i - J_f| \leq J \leq |J_i + J_f|$ transferred to the daughter nucleus. Allowed and unique transitions involve only single β moments, while the β rates of the nonunique decays are determined by incoherent (and mutually cancelling) contribution of different β moments. Besides, for $J = 0, 1$ transitions, the relativistic vector operator α and axial charge operator γ_5 should be included alongside with the space-like operators. This brings serious difficulties. First, it was shown on the basis of the chiral symmetry and soft-pion limit that $\langle\gamma_5\rangle$ vertex is amplified in the nuclear medium due to the meson-exchange currents and the effective NN interactions [124] but the details have not been well established. Second, in a nonrelativistic limit the former corresponds to the velocity-dependent fields $\mathbf{P}/2M$ and $\boldsymbol{\sigma}\mathbf{P}/2M$, where $P = P_i + P_f$ is the total momentum transferred to the nucleus, and M is the bare nucleon mass. Thus, the consistent treatment of the medium induced fields requires taking into account the velocity-dependent and two-body spin-orbit effective NN interactions. This complicates the QRPA equations substantially.

A convenient approximation to be used in global calculations of total half-lives is to replace α, γ_5 by the space-dependent fields. The exact nonrelativistic relation for the matrix element of the time-like operator

$$\langle\alpha\rangle = \xi/\lambda_e \cdot \Lambda_1 \langle i\mathbf{r}\rangle \tag{39}$$

can be applied which reflects the conservation of the nuclear vector current (NVC). In a fully self-consistent approach a precise cancellation of all the terms except the averaged Coulomb potential takes place, thus the translation factor Λ_1 reads:

$$\xi\Lambda_1 = \omega_{if} + \bar{u_C}. \tag{40}$$

For the operator γ_5 and its space-like counterpart $\boldsymbol{\sigma}\mathbf{r}$, no analogous exact relation exists due to the partial conservation of the axial current. The self-consistent FFS sum rule approach [130] can be used to approximate the operator γ_5 by the space-like operator $\boldsymbol{\sigma}\mathbf{r}$ taking into account the medium corrections [126]. With the resulting set of the space-dependent external fields, the large-scale calculations of the β-decay half-lives are feasible. For the nuclei at $N = 50$, 82, 126, the first systematic calculations including the contribution of the GT and FF transitions

on the same microscopic footing have been performed within the self-consistent HFBCS + CQRPA in [125, 126].

The only attempt of fully self-consistent HFB + QRPA calculation has been done in [127] who used the Skyrme energy-density functional to estimate the allowed β^--decay rates of spherical even–even semimagic nuclides with $N = 50$, 82, and 126. In [127] the HFB + QRPA equations are treated on the finite basis of the canonical states. The advantage of the approach is using the same Skyrme (SkP) effective NN interaction in both the ph and pp channels. However, the value of the Landau–Migdal spin-isospin parameter g' derived from the SkP force is much lower than the empirical value. Consequently, the GTR position is predicted to be lower by about 2 to 3 MeV than experimental data. To compensate for this deficiency in the half-life calculations, a rather strong A-dependent pp interaction is considered. For practical astrophysical purposes, it will cause problems in estimating the decay properties and ν_e-capture-rates of thousands of nuclei. (A detailed study of the above-mentioned «g'-problem» in the fully self-consistent calculations can be found in [128].) For the β-decay half-lives, the results by [127] are close to those of [121], provided the same effective pp interaction and quenching factor are adopted.

To conclude the overview of the microscopic models for nuclear weak-interaction rates, let us also mention their main deficiencies which may influence the astrophysical predictions. The most important one concerns the pairing interaction of use in the ground state masses calculations and in dynamics calculations of the β-strength function. The point at weakness here is the lack of universal parametrization of the pairing interaction. Moreover, as both the BCS and HFB calculations with commonly used δ-function pairing diverge respective to the active space size, they need to be complemented with a cut-off in the single-particle space (for BCS) or in the quasiparticle space (for HFB). This cut-off could be considered, as purely computational procedure, however it effectively accounts for missed physical mechanism of phonon exchange providing the long-range behavior of the pairing interaction. For density-dependent pairing a local cut-off treatment of the pairing energy density [39] or a pairing regularization suggested recently in [135] helps to avoid the above-mentioned «nonconvergence»-problem. Another unsatisfactory feature of the BCS pairing — the existence of nonphysical neutron gas very close to the neutron drip-line [134] — is removed within the HFB which properly takes into account the scattering of the nucleon pairs to continuum.

A nonuniversal treatment of the pairing force influences the predictions of both the ground state properties (nuclear masses) and β-decay rates. An interplay of the deformation and nuclear pairing effects is responsible for the quenching of single-particle spectra gaps at canonical neutron magic numbers in very neutron-rich nuclei (shell gap quenching) [138]. A simple signature of neutron shell closures related to the nuclear masses is given by the two-nucleon shell gap

$\delta(Z,N) = S_{2n}(Z,N+2) - S_{2n}(Z,N)$. The measured nuclear masses at $N =$ 20, 28, and 50 show that the corresponding magic gaps $\delta(Z,N)$ decrease with decreasing Z — an indication of the quenching which sets in near the neutron drip-line. For $N = 82$, 126, however, no definite conclusion can be drawn from the available experimental data. Clearly, all the existing theoretical predictions of nuclear masses depend crucially on the adopted concept of nuclear pairing.

The ground state pairing has been shown to modify the β-strength function and, thus total β-decay half-lives [113]. Due to the additional dependence of the phase space on the S_n value, the β-delayed neutron emission is even more sensitive to pairing. The BCS-based estimate of this effect has been done in [136] where the constant pairing has been used, and the case of ^{137}I nucleus with a small $(Q_\beta - S_n)$-window has been considered. The systematic study of the impact of the density-dependent pairing on the total β-decay half-lives and delayed-neutron branchings (P_n) in very neutron-rich nuclei is of importance.

So far, the microscopic large-scale calculations of masses [30, 31, 39] and weak interaction rates [113, 121, 125, 127] have used phenomenological energy-density functionals corresponding to the energy-independent effective NN interactions. One of the alternatives is to construct the energy-dependent effective NN interaction from the vacuum NN-scattering amplitude. The calculation of the ground-state masses [137] using the quasiparticle Lagrangian version of the self-consistent FFS [36] with energy-dependent effective NN interaction shows that for small values of the neutron chemical potential, the parameters of the effective NN interaction, and consequently the self-consistent mean fields, vary strongly. As a result, the neutron drip-line position shifts to very large values of the neutron excess [137]. With the «modified» neutron drip-line, a role of forbidden decays may increase, as the driving operators contain the factor r/R_0. In this situation, a possible existence of superallowed Fermi, as well as accelerated Gamow–Teller and first-forbidden β decays may be anticipated in doubly-magic drip-line systems.

In spite of the remaining difficulties, an important progress has been achieved in the step-by-step transition from the phenomenological models towards to the self-consistent description and prediction of the β properties. In the future, a substantially improved spherical QRPA approach can possibly be used for practical applications. Based on the self-consistent predictions for the ground state properties within the coordinate-space HFB [39], the excited states can be treated in the continuum linear response theory [131, 132]. The QRPA based on the canonical basis of the relativistic HFB has been developed in [133]. For the ground state pairing, well defined basis regularization schemes can be used [39, 135]. Though the QRPA models used for large-scale calculations of the strength functions have considered so far simple ph configurations, this limitation is not a principal one and can be removed. A fully self-consistent Hartree–Fock–Bogoliubov (HFB) or even HFBCS plus CQRPA approach applicable to large-

scale calculations of the ground state and β-decay properties of deformed nuclei has not been achieved yet (mainly for technical complexity and computational limitations).

For readers convenience, the existing microscopic global approaches to the weak rates are summarized in Table 1 which contains a short description of the methods, their applicability limits and some important details of the calculations. Let us now discuss the performance of the microscopic β-decay models for the r-process relevant nuclei. Below, we give a detailed comparison between the different approaches and available experimental data. In comparing the results, it should be clearly realized how the model parameters have been found: either by a direct local fit to the experimentally available half-lives, or by a global fit of the (universal) NN-interaction parameters to the other spin-isospin properties (like energy positions of the spin-isospin resonances, magnetic moments, ...).

Table 1. **The global microscopic approaches to the weak interaction rates**

Method	The ground state	NN interaction	Details
FRDM + RPA [99]	Empirical potential, BCS + folded Yukawa	ph: separable pp: no	$T_{1/2}$, (GT-approximation) all A no direct fitting to the $T_{1/2}$
BCS + QRPA [105]	Empirical potential, BCS + Nillson	ph: separable pp: separable	$T_{1/2}$, (GT) all A local fitting to the $T_{1/2}$
SM [88]	$0-\hbar\omega$	pf-shell KB3	$T_{1/2}$, (GT) $N = 50, 82, 126$ local fitting of G_A/G_V
WS + RPA [158]	Empirical potential, Woods–Saxon	ph: δ-force	σ_{ν_e} local fitting of the WS potential
ETFSI + CQRPA [121]	Self-consistent, Skyrme-ETFSI	ph: $\delta+\pi$ pp: δ	$T_{1/2}$, (GT) 800 quasi-spherical nuclei ($\beta_2 \leq 0.1$) σ_{ν_e}, $\sigma_{\bar{\nu}_e}$ all A no direct fitting to the $T_{1/2}$
DF + CQRPA [113]	Self-consistent, DF3 [39, 113]	ph: $\delta+\pi+\rho$ pp: density-dep.	$T_{1/2}$, (GT + FF) 800 quasi-spherical nuclei ($\beta_2 \leq 0.1$) no direct fitting to the $T_{1/2}$
HFB + QRPA [127]	Self-consistent, Skyrme	Self-consistent, Skyrme	$T_{1/2}$, (GT) $N = 50, 82, 126$ local fitting of the pp interaction

2.4. GT and FF Decays Near the Closed Shells. Of course, the theoretical studies for nuclei far off stability need a rigid experimental verification. Experiments using a new generation of the radioactive ion beam facilities are crucial in validating the existing theories. Great attention has been paid to the nuclei near the closed shells at $Z = 28$, $N = 50$; $Z = 50$, $N = 82$; and $Z = 82$, $N = 126$ providing an important benchmarks for theoretical models. The high precision data for short-lived Ni isotopes near ^{78}Ni [139], $^{121-129}$Ag isotopes [140] and $^{133-137}$Sn [142] have been measured at RILIS (CERN), which benefits from the high isotopic and isobaric selectivity reached by a laser ion source and by mass spectroscopy, respectively. The current experimental studies in the neutron-rich and neutron-deficient lead regions [143, 144] are very important for studying the nuclear structure at extreme neutron-proton asymmetry, as well as for elucidating the weak interaction and β-decay theories.

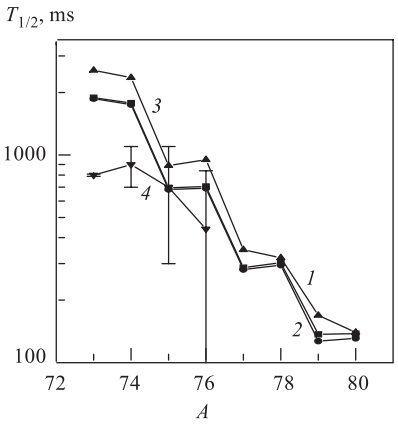

Fig. 8. The experimental β-decay half-lives for the Ni isotopes compared to the calculations with the DF3 and Msk7 g. s. description ($Q = 0.81$): ■, curve *1* — DF3 + CQRPA for allowed transitions; ●, curve *2* — DF3 + CQRPA for allowed and first-forbidden transitions; ▲, curve *3* — MSk7 + CQRPA for allowed transitions; ▼, curve *4* — experimental data from [139]

The neutron-rich nuclei near the closed-shells at $N = 50$, 82, and 126 provide a clear case for the application of the CQRPA model, for a comparison of different methods, and for experimental checks. First, they are not extreme dripline systems ($S_n \approx 2.0{-}3.0$ MeV $> \Delta$, where Δ is the pairing potential), therefore an application of the mean-field approach should not yield too large errors. Second, most of these nuclei are spherical, hence their β-decay half-lives are very sensitive to nuclear structure effects. Third, the nuclei with $Z \approx 28$ near ^{78}Ni and $Z \approx 50$ near ^{132}Sn, as well as the ones near $Z \approx 60{-}80$ at $N = 126$ undergo high-energy GT and/or FF β decays. In these conditions, the spherical, $1p1h$-QRPA approaches accounting for the allowed and FF transitions should have a reasonable accuracy in predicting the β-decay half-lives.

Though the «thumb rule» is that the β-decay half-lives become longer as closed (sub)shells are approached, the $T_{1/2}$ are found to be sensitive to the specific shell sequence and the partial occupancy of the proton orbital which is mainly due to the interplay of the GT and high-energy FF transitions near the specific shell closures. It can be well seen when analyzing the evolution of the β-decay patterns in the nuclei from $N \approx 50$; $Z < 28$, $Z \gtrsim 28$ regions (for instance in Fe, Co

isotopes and Ni, Cu isotopes) and from $N \approx 82$; $Z < 50$, $Z > 50$ regions (for instance in Ag, Cd isotopes and Sn, Sb isotopes).

According to the available experimental [139] and predicted [99, 121] decay schemes, the nuclei in the vicinity of $Z = 28$, $N = 50$ shell sequence undergo fast high-energy GT decays which are built mainly on the simple shell-model configurations $\nu 1f_{7/2,5/2} \to \pi 1f_{7/2,5/2}$ and $\nu 1g_{9/2} \to \pi 1g_{9/2}$. The first-forbidden decays are due mainly to the $\nu 1g_{9/2} \to \pi 1f_{7/2}$ and $\nu 1f_{5/2} \to \pi 1d_{5/2}$ transitions with the energies close to that of the GT decays. In Fig. 8 we show our predictions for Ni isotopes obtained including the first-forbidden decays. Two different ground state descriptions are used, the DF3 and MSk7-based calculations being in better agreement with the experimental data than our previous ETFSI results [121]. Note that this improvement results, in part, from the reduction of the half-lives caused by the stronger effective pp interaction used in the present calculations. It is seen from Fig. 8 that the first-forbidden transitions are of little effect for nuclei near $Z = 28$, $N = 50$. In this region, a number of GT and FF transitions with comparable energies exist, with the GT decay channel dominance. It is of importance that the high-energy GT transitions exist both at $Z < 28$ and at $Z = 28{-}29$. Thus, even when the $\pi 1f_{7/2}$ orbital is completely blocked, still many high-energy GT transitions remain open.

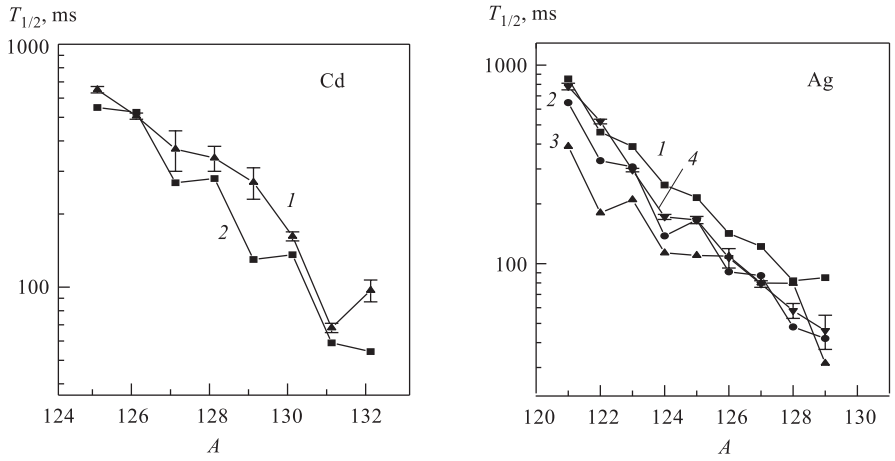

Fig. 9. The experimental β-decay half-lives for the Cd isotopes taken from the NUBASE [100,141] (▲, curve *1*) compared to the DF3 + CQRPA calculations (■, curve *2*)

Fig. 10. The calculated total half-lives for the Ag isotopes: ■, curve *1* — DF3 + CQRPA for pure GT decays; •, curve *2* — DF3 + CQRPA [125,126] with the GT and FF transitions included; ▲, curve *3* — the results by Hybrid-model by [104] with the GT decays included within the RPA and FF decays within the «gross theory». The experimental (▼, curve *4*) and estimated data are from NUBASE [100, 140]

Unlike $Z \approx 28$ region, for the $Z < 50$, $N \approx 82$ nuclei, the high-energy GT transitions to the major $1\pi g_{9/2}$-orbital dominate the total half-life. Our calculations including the FF transitions [125, 126] show a moderate influence of the FF transitions for nuclei in $Z < 50$, $N = 82$ region. As is seen from Figs. 9, 10, the FF transitions provide a factor of 1.5–2 acceleration of the β decays for the Cd and Ag isotopes. By contrast, in the region with $Z \gtrsim 50$, $N \approx 82$, the high-energy FF transitions are found to give a stronger contribution to the total half-lives than the low-energy GT decays [125, 126, 129, 142]. Indeed, for $Z = 50{-}51$, $N \approx 82$ nuclei, the only high-energy GT β transition involving the major $1\pi g_{9/2}$ orbital is fully blocked. Due to the phase space effect, the high-energy forbidden transitions related to the $\nu 2f_{7/2} \rightarrow \pi 1g_{7/2}$, $\nu f_{7/2} \rightarrow \pi 2d_{5/2}$ configurations dominate the total half-life. For nuclei with $Z \geq 52$ and $N \approx 82$, the $1\pi g_{9/2}$ orbital is freed due to pairing correlations but the related GT strength is reduced by the factor $(1 - v^2_{1\pi g_{9/2}})$.

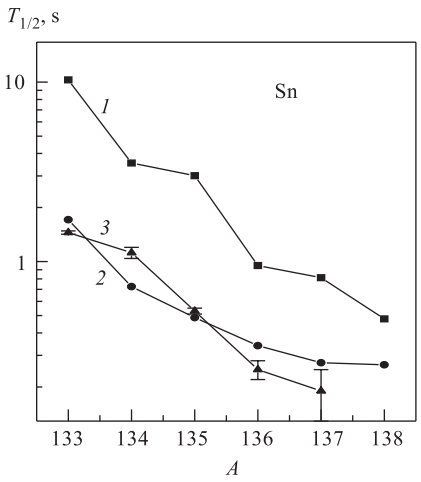

Fig. 11. The calculated total half-lives for the Sn isotopes: ■, curve *1* — FRDM + RPA for pure GT decay [99]; ●, curve *2* — DF3 + CQRPA with the GT and FF decays included [126]; ▲, curve *3* — experimental data are from [142]

Earlier measurements in the ^{133,134}Sn, as well as recent RILIS CERN experiments in $^{133-137}$Sn demonstrate clearly the existence of the high-energy FF and low-energy GT transitions. For the Sn isotopes (Fig. 11), the FRDM calculations [99] performed in the allowed transition approximation strongly overestimate the experimental half-lives. Inclusion of the FF transitions brings the calculated half-lives into a fairly good agreement of our calculations with the experiment (Fig. 11), and shows that the Coulomb decay mechanism dominates in these nuclei.

2.5. Model Predictions Near $N = 50, 82, 126$. Now let us turn to the calculations for the r-process relevant nuclei near the $N = 50$, 82, 126 closed neutron shells. The HFBCS + CQRPA results [125, 126] show that the effect of FF transitions is small in $Z \approx 28$, $N = 50$ region (notice that spherical approach may fail in this region). For nuclei with $N = 82$, $Z < 50$, the experimental benchmarks at ^{129}Ag, ^{130}Cd, ^{131}In were obtained in a series of RIB experiments at RILIS CERN [145]. It is of interest to confront these experimental data with the predictions made within the different theoretical approaches. The FRDM-RPA

calculations (not shown in Fig. 12), with a nonconsistent treatment of the ground state properties and ignoring the pp-effective NN interaction, give an odd–even effects which are not supported by the existing experimental data [145]. In the $N = 82$, $Z < 50$ region, the ETFSI calculations [121] (also not shown) overestimate the experimental half-lives by about a factor of two. It is mainly due to the pp-interaction strength g'_ξ used in [121] which was extracted from the old experimental data on the (p, n)- and (n, p)-reactions spectra [146], the latest TRIUMF experiments [147] leading to a higher value of g'_ξ. The results of systematic calculations of the β-decay half-lives [125] with a stronger pp interaction, as well as with the GT and FF transitions taken into account (Fig. 12) show a much better agreement with available experimental data than the previous ETFSI results [121]. The calculations including the FF decays show a slight odd–even effect which is in agreement with available experimental data.

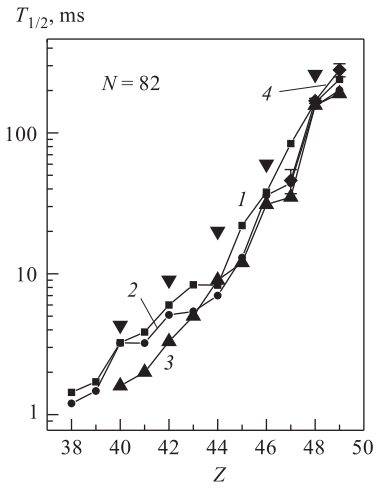

Fig. 12. The total half-lives for the $N = 82$, $Z < 50$ isotones: ■, curve *1* — DF3 + CQPA ($Q = 0.81$) — with only GT transitions included; •, curve *2* — DF3 + CQRPA with the GT and FF transition included; ▲, curve *3* — SM — shell-model results for pure GT decay [88] ($Q = 0.55$); ▼ — HFB — results for pure GT decay [127] ($Q = 0.64$). The experimental data (♦, curve *4*) are from [100]

In Fig. 12, we compare also the results of the DF + CQRPA [125, 126] with the HFB calculations [127]. These results were obtained with one and the same pp-interaction strength g'_ξ but with different quenching ($Q = 0.81$ and 0.64, respectively). In both the approaches the quenching factor is the same which enters the Ikeda sum rule. Thus, the lower quenching of $Q = 0.81$ would drive the HFB results in closer agreement with our results and the experimental data. Note that for the shell-model calculations [88], the quenching factor Q is related to the model space of use, but it is not directly connected to the quenching of the Ikeda sum rule. However, reducing the quenching and inclusion of the FF transitions would drive the results of [88] below the experimental data (Fig. 12).

In contrast, in the region near $Z \approx 60-75$ and $N = 126$, the role of the FF decays is found to be decisive. These nuclei undergo high-energy FF decays related to the $\nu 1i_{13/2} \to \pi 1h_{11/2}$ configuration. At the same time, the unperturbed β-decay energy of the main GT decay configuration $\nu 1i_{13/2} \to \pi 1i_{11/2}$ is low (about 1 MeV). Thus, it is clearly seen in Fig. 13 that the behavior of the

half-lives for the GT and GT + FF transitions reflects the blocking of the $1\pi g_{9/2}$ and $1\pi h_{11/2}$ levels with increasing Z.

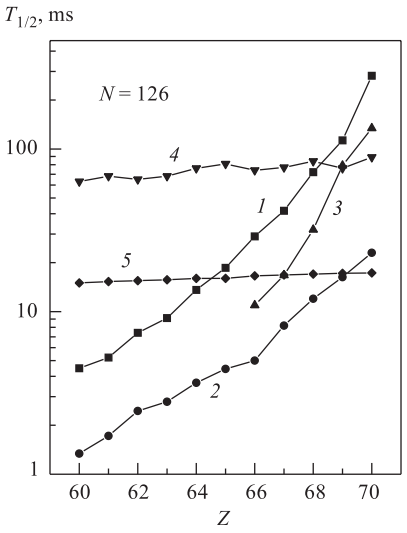

Fig. 13. The total half-lives for the $N = 126$ chain: ■, curve *1* — DF3 + CQRPA calculation for the GT decay only; •, curve *2* — DF3 + CQRPA calculation with the GT + FF decays included; ▲, curve *3* — the shell-model calculation [89]. The half-lives against (ν_e, e^-)-capture (calculated with $L = 10^{51}$ erg $\cdot$ s^{-1}, $R = 100$ km) are also given for $T_\nu = 4$ MeV [121] (▼, curve *4*) and $T_\nu = 8$ MeV (⧫, curve *5*) [158]

In Fig. 13 a comparison is presented with the shell-model calculations [88] performed in the allowed transition approximation and with $Q = 0.55$. It is seen that the inclusion of the FF transitions results in noticeably shorter half-lives in the $N = 126$ region. The difference with the allowed-transition approximation amounts to typically a factor of 5 to 10, and is more pronounced for heavier nuclei approaching the closed proton shell at $Z = 82$. Note that the shell-model half-lives of [89] would be shorter if the FF decays were included and/or a smaller quenching used. The shorter half-lives predicted for $N = 126$ should have the implications on the r-process nucleosynthesis in this region (see discussion in the next section).

Though, it is hard to experimentally check these theoretical predictions at the time being, a comparison can be performed with the current experimental data for the neutron-rich nuclei in the region «east» of ^{208}Pb [143, 144]. In Fig. 14, the experimental half-lives in the Bi isotopes [100, 143, 144] are confronted to the predictions from different global approaches [86, 99, 104, 126, 127]. The total half-lives for the GT decay calculated within the FRDM + RPA model [99] overestimate the experimental ones by orders of magnitude. The scale of the odd-even effects predicted by this model is generally too large because of the nonconsistent treatment of the ground state properties and pairing correlations, and also due to the pn-effective interaction is not included in [99].

The results of statistical calculations [86] with a parametric description of the forbidden transitions, vary significantly from the odd-A to even nuclei. Also shown in Fig. 14 are the results from the recent «micro-statistical» version of the FRDM model [104]. This model provides shorter total half-lives than the ones calculated for the GT decay in [99]. However, a strong renormalization of the GT half-lives, for example in ^{216}Bi, is hard to explain from microscopic arguments.

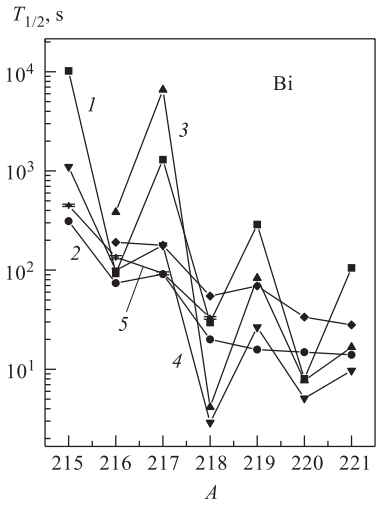

Fig. 14. The β-decay half-lives for Bi isotopes predicted from different approaches: ■, curve *1* — statistical «gross-theory» with the GT and FF transitions included in a parametric way [86]; •, curve *2* — DF3 + CQRPA with the GT and FF decays included microscopically [126]; ▲, curve *3* — FRDM + RPA for pure GT decay [99]; ▼, curve *4* — the hybrid-model [104] with GT decays included in the RPA and FF decays in the «gross-theory»; +, curve *5* — Nillson + QRPA for pure GT decays [105]. The experimental data are taken from the NUBASE [100] and recent measurements by Leuven group [143, 144]

It may well come from the inconsistency in the microscopic and «gross-theory» inputs which is unavoidable in the hybrid models.

The QRPA calculations by [105] are over-parametrized compared to the BCS-RPA calculations by [99], as the strengths of the separable ph and pp NN interactions are (locally) fitted to the experimentally known half-lives at each isotopic chain which is a purely empirical procedure. On the other hand, as the odd–even behavior of the half-lives calculated in [105] is reasonable (the $T = 0$ paring has been included), such a procedure may in some cases give a sound extrapolation to the closest experimentally unknown nuclei. However, as the FF transitions have not been included, it is quite natural that the calculations by [105] overestimate the experimental half-lives in the region of Bi isotopes.

Our calculated half-lives show a fairly regular behavior with some underestimate of the experimental total half-lives (Fig. 14). The calculation may still be oversimplified in the specific region «east» of ^{208}Pb, especially if the $\Delta J = 0$ transitions dominate in the decay schemes. This is mainly due to the neglect of the velocity-dependent terms in the effective NN interaction and to the use of the Coulomb (ξ) approximation. However, in general, the results are in a qualitative agreement with available experimental data on total half-lives. Thus, the calculations may provide a guidance for new experiments in this region of the nuclear chart.

2.6. Neutrino Capture Rates. In neutrino-rich environments, like in the so-called neutrino-driven wind characterizing the neutrino heated ejecta at the surface of the proto-neutron star after the core collapse of a type II supernova [76, 77], the neutrino interaction with the stellar material must be taken into account. The universality of the weak interaction and existence of weak equilibrium in the

core impose a rough equipartition of energy between the $\nu_x, x = \mu, \tau$ and $\bar{\nu}_e, \nu_e$ neutrino species. In contrast, a subsequent decoupling of the neutrinos from the matter is strongly flavor dependent. The $\nu_x, \bar{\nu}_x$ species does not interact with the nucleons of the proto-neutron star via charged-current reactions, their cross sections for scattering off the electrons are also smaller than for ν_e and $\bar{\nu}_e$ species. Thus, the $\nu_x, \bar{\nu}_x$ decouple deepest in the proto-neutron star (at smaller radius and higher temperatures) and have higher energies than electron neutrinos and antineutrinos. As the matter near the surface of proton-neutron star is partially deleptonized and neutron-rich, the ν_e which are captured by the neutrons are last to decouple. Hence, they have the smaller energy than $\bar{\nu}_e$ which interact with protons. Such energy hierarchy is established near the surface of nascent neutron star (the so-called neutrinosphere) after the neutrinos have been diffused out the core. The transport calculations by [148] correspond to the following hierarchy of average neutrino energies $\bar{E}_{\nu_e} \approx 11 < \bar{E}_{\bar{\nu}_e} \approx 16 < \bar{E}_{\nu_{\mu,\tau}} \approx \bar{E}_{\bar{\nu}_{\mu,\tau}} \approx 25$ MeV.

To estimate the chemical transmutation in such a neutrino-rich environment, the ν captures on heavy nuclei must be determined. These include the charged and neutral current interactions which need to be estimated consistently within the same framework as the nuclear masses and β-decay rates. The spectrum-averaged cross section of the electron neutrino capture in the stellar environment reads

$$\langle \sigma_\nu \rangle = A^{-1} \int_{E_{\rm th}}^{E_\nu^{\rm max}} \phi(E_\nu)\ \sigma_\nu(E_\nu) dE_\nu, \tag{41}$$

where $E_{\rm th} = |\Delta M_{Z,Z+1}|$ is the reaction energy threshold for stable nuclei ($E_{\rm th} = 0$, otherwise). The neutrino energy spectrum $\phi(E_\nu)$ is taken as

$$\phi(E_\nu) = C\ \frac{E_\nu^2}{T_\nu^3\ \exp\left[(E_\nu/T_\nu) - \alpha\right] + 1}. \tag{42}$$

T_ν is the neutrino temperature; C normalizes the spectrum to unit flux; $\alpha = 0$ corresponds to a black body spectrum; $\alpha = 3$ has been derived from the transport calculations [148].

Electron neutrino capture $\nu_e + A_Z(J^\pi) \rightarrow e^- + A_{Z+1}(J'^{\pi'})$ which takes place through weak charged current can be seen as an inelastic scattering process with a discrete energy spectrum of the emitted electron

$$E_e = E_\nu + Q - \omega_x + m_e c^2, \tag{43}$$

here and below the notation $Q = \Delta M_{Z,Z+1}$ is used for convenience. The neutrino-energy-dependent cross section is derived within the standard semi-leptonic scattering framework [149]. The expression for the cross section of inclusive reaction $\nu_l + |i\rangle = l^- + |f\rangle$ reads

$$\sigma_\nu = \int d^3 p_l \delta(E_l + E_f - E_i - E_\nu) |\langle l(p_l)|H_{\rm eff}|\nu(p_\nu)\rangle|^2, \tag{44}$$

where E_ν is the incident neutrino energy; E_l, p_l are the final energy and momentum of the lepton ($l = e,\ \mu$); $E_i(E_f)$ is the energy of the initial (final) nuclear state. We will follow [150], where Eq. (44) has a form convenient for using the β-like strength function formalism. The effective single-particle Hamiltonian is derived by carrying out the Foldy–Wouthausen transformation and retaining terms up to order $(|q|/M)^3$ (M is the nucleon mass and q is the momentum transfer), the terms with P_N/M corresponding to the nucleon motion in the initial states are omitted. The finite momentum transfer dependence of the cross section is of importance for the high supernova neutrino temperatures.

If the nuclear recoil effects are ignored, one has

$$\sigma = \sigma_0 \int d\omega p_l E_l F(Z_f, E_l) \int_{-1}^{1} d(\cos(\theta)) S_\beta(q, \omega), \tag{45}$$

where $\sigma_0 = G^2/2\pi\cos^2(\theta_C)$; G and θ_C are the Fermi constant of universal weak interaction and Cabibbo angle; P_l and E_l are the momenta and energies of outgoing leptons, θ being the angle between the momenta of the lepton and the neutrino; $\omega = E_f - E_i$ is the energy of nuclear transition; $F(Z_f, E_l)$ is the Fermi function taking into account the Coulomb distortion of the outgoing lepton wave function due to its final state interaction with the daughter nuclei with the charge Z_f. (For high-energy ν_μ neutrinos, the «effective momentum approximation» [159] is used, and for the case of ν_e, the interpolation between this and standard Fermi approximation can be used [158].) The nuclear structure effects are incorporated to the strength function $S_\beta(q, \omega)$ which in the notations of [150] reads

$$S_\beta(q, \omega) = M_F S_F + M_{G0} S_{G0} + M_{G2} \Lambda, \tag{46}$$

where the kinematics coefficients M_i depend on the four-momentum transfer to the nucleus and standard nucleon form factors entering the H_{eff} in the case when the second-class current form factors are ignored. The strength functions S_F and S_{G0} are the sums of nuclear responses to the external fields of the isospin type $V_0 \sim \tau_- j_l(qr_k) Y_l(\hat{r}_k)$ and of spin-isospin type $V_0 \sim \tau_- j_l(qr_k)[\sigma Y_l(\hat{r}_k)]^J$, while Λ stands for spin-isospin interference term. The transition operators in Eq. (46) that satisfy the selection rules $\Delta J = 0, 1$; $\Delta\pi = +$ correspond to the allowed-type operators; while all the others, to the forbidden type. In the original scheme proposed by [150] the single-particle response functions have been used. However, the formalism allows for including the medium effects through the corresponding strength functions calculated in the RPA or QRPA framework (for details see [150, 151]).

In the low energy limit with $q \to 0$, Eqs. (44), (45) are reduced to a familiar expression of the allowed transition approximation which is applicable for low

neutrino temperatures

$$\sigma_\nu(E_\nu) = \frac{1}{\pi\hbar^4 c^3} \times \\ \times \int_0^{E_\nu+Q} p_e E_e F(\pm Z, A, E_e) \left[G_V^2 S_F(\omega_x) + G_A^2 S_{GT}(\omega_x)\right] d\omega_x. \quad (47)$$

The plus sign in the Fermi function refers to the ν-capture and S_F (S_{GT}) is the strength function of the Fermi (Gamow–Teller) transition. In Eq. (47), the integration over the excitation energy in the daughter nucleus $\omega_x = Q - \omega$ runs over all energetically possible final states in the daughter nucleus. For stable nuclei ($Q < 0$), the ν-induced excitation of the states in the daughter nucleus corresponds to nuclear transitions with a negative Q-value ($\omega < m_e c^2$). For unstable nuclei ($Q > 0$), we consider the contributions of both the ν-induced excitations ($\omega < m_e c^2$) and the ν-mediated de-excitations ($\omega \geq m_e c^2$), where lepton final states correspond to nuclear transitions to the discrete states in the daughter nucleus with a positive Q-value.

Finally, the flux-dependent neutrino capture rate at the distance R from the centre of neutron star can be estimated as (e. g., [153])

$$\Lambda_\nu \approx 4.97 \left(\frac{L_\nu}{10^{51}\ \text{erg}\cdot\text{s}^{-1}}\right)\left(\frac{\text{MeV}}{\langle E_\nu\rangle}\right)\left(\frac{100\ \text{km}}{R}\right)\left(\frac{\langle\sigma_\nu\rangle}{10^{-41}\ \text{cm}^2}\right)\ \text{s}^{-1}, \quad (48)$$

where L_ν is the neutrino luminosity. The average electron neutrino energy for the distribution given in Eq. (42) is $\langle E_\nu\rangle = 3.15T_\nu$ for $\alpha = 0$ and $\langle E_\nu\rangle = 3.99T_\nu$ for $\alpha = 3$. It is seen that the neutrino capture rate is directly proportional to the neutrino flux streaming out of the proton-neutron star. Therefore it is R-dependent quantity, unlike the β-decay rate.

The detailed and physically transparent consideration of the physics of ν_e and $\bar{\nu}_e$ captures on heavy nuclei in the context of the post-core bounce supernova environment can be found in [157]. Due to the relatively high mean energies of supernova neutrinos, the main contribution to the spectrum-averaged cross sections comes from the IAS, GT and $\Delta L = 1$ charge-exchange resonances. However, the charge-exchange strength functions are treated in [157] within the «gross-theory», thus remaining valid for nuclei relatively close to the β-stability line. Moreover, the contribution of low-lying «pygmy» resonances for stable nuclei has been ignored and ν-mediated de-excitation in unstable nuclei neglected. For stable nuclei, a low-lying pygmy-resonance contribution to the $(\nu - A)$-capture cross sections has been considered by [154] making use of a schematic three-level FFS-based model. A calculation of the neutrino capture rates in the neutrino detector nuclei has been performed in the optical-shell model [155] and self-consistent model based on the energy-density functional and CQRPA [112].

In [151], the charged-current neutrino reactions on ^{12}C, ^{16}O, and ^{208}Pb have been considered in the formalism of [150] with the β-strength functions calculated from the RPA, QRPA, and shell-model. The RPA calculations of the $(\nu_e - A)$ cross sections with the GT and FF transitions taken into account have been performed in [156] for three representative nuclei near $N = 50$, 82, 126.

Within the same ETFSI + CQRPA framework, as for the β-decay rates, the model for charged-current neutrino capture has been developed in [122]. A corresponding large-scale calculation of the neutrino energy-dependent and spectra averaged cross sections has been performed for all stable and unstable neutron-rich nuclei with $26 < Z < 92$ and neutron numbers from $N = Z + 1$ to the neutron drip-line in [121] (see also www.astro.ulb.ac.be). In the ETFSI + CQRPA approach to the charged-current neutrino capture, the GT strength function is calculated for the excitation energy range from the ground state of the daughter nucleus up to about 40 MeV. The IAS energies are taken from the experimental systematics of Coulomb displacement energies [161]. The Fermi strength included in the IAS of the daughter nucleus is taken as $M_F^2 = N - Z$.

Let us discuss in more detail the neutrino capture cross sections calculated in the allowed transitions approximation. The total cross sections averaged over neutrino spectrum [148] with $T = 4$ MeV are shown with their partial components for the Ni, Sn, and Pb-isotopic chains in Fig. 15. In stable nuclei, the IAS and ν-induced excitation components of the total cross section increase with $N - Z$ due to the corresponding shift of the IAS and GT resonance (GTR) down in energy and towards the maximum of the neutrino energy spectrum (note that the correct reference energy here is the one respective to the parent nucleus ground state, and not the excitation energy in the daughter nucleus). For stable nuclei, the contribution of the neutrino excitation of the low energy states in the daughter nucleus cannot be neglected. Such a contribution is responsible for the systematic odd–even effect in the total cross section, as illustrated in Fig. 15.

In unstable nuclei, at increasing neutron excesses, the IAS and GT-excitation contributions to the cross section become rather smooth and insensitive to odd–even nuclear mass differences (the capture process is of no-threshold type). At relatively small charge numbers Z, the GT-excitation component may even decrease with increasing neutron numbers, at least if the super-allowed GTR is energetically possible (note that for these nuclei the empirical systematics of the IAS energy may fail). At the same time, the GT de-excitation component of the cross section in unstable nuclei increases with neutron excesses, as the Q_β value (and available phase-space) becomes larger. For relatively small Z, the de-excitation part of the total cross section cannot be neglected. As is seen in Fig. 15, for Ni isotopes, it exceeds the IAS contribution well before the neutron drip-line is reached. This is mainly due to the increasing portion of the GT sum rule shifted within the Q_β window at increasing $N - Z$ values. The impact of the de-excitation component is smaller for heavy isotopic chains ($Z > 50$) for

which the super-allowed GT transition is not possible for neutron-stable nuclei. For heavy nuclei, like Pb isotopes (Fig. 15, *c*), these predictions agree well with the schematic estimate of the de-excitation contribution by [157]. In the ^{132}Sn region, the calculated neutrino capture rates [121] are rather close to the one derived by the shell-model calculations [153].

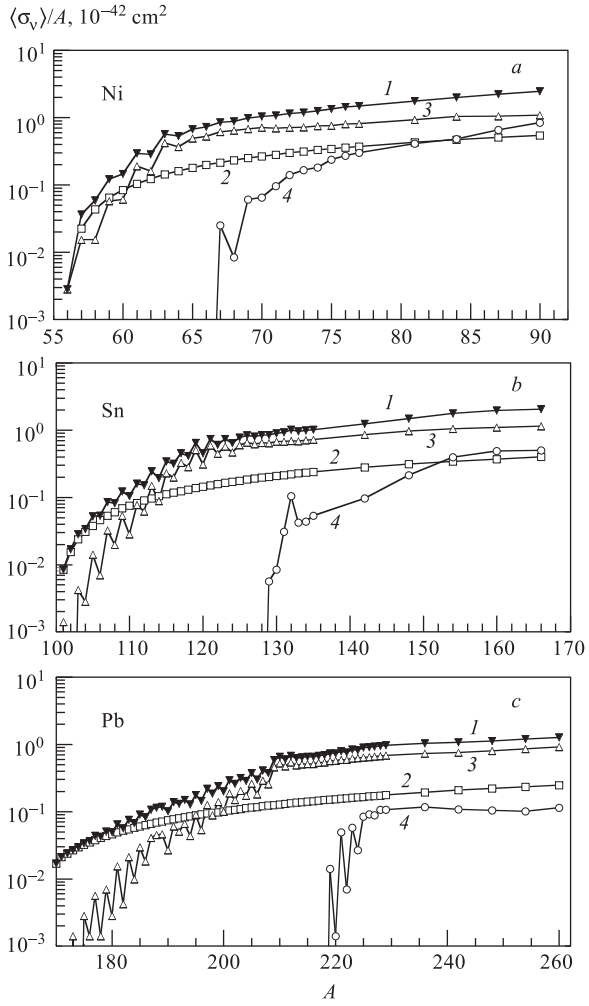

Fig. 15. Reduced total neutrino capture cross sections (tot.) (▼, curve *1*) averaged over neutrino spectrum [148] with $T = 4$ MeV for Ni (*a*), Sn (*b*) and Pb-isotopic chains (*c*). Also shown are their partial components of the IAS excitation (IAS) (□, curve *2*), ν-induced excitation (gt $>$) (△, curve *3*) and de-excitation (gt $<$) (○, curve *4*)

An extensive calculation of the charged-current and neutral current inelastic neutrino scattering cross sections has been performed in [158, 160] making use of the standard Walecka formalizm employing the momentum dependent external field operators. The neutrino scattering cross sections are calculated assuming the neutrino energy distributions with chemical potential of $\alpha = 0$ and $\alpha = 3$ and for each of the values, temperatures $T_\nu = 2.75$ to 10 MeV. This grid of (α, T) has been used to study the effect of neutrino oscillations. To find the strength functions of the IAS, GT, and FF states, the RPA problem is solved using the restricted basis and the quenching factor $Q = 0.49$ taken from the shell-model calculations. The single-particle energies are obtained for an empirical Wood–Saxon potential with parameters (locally) adjusted to the nucleon separation energies given by the mass compilation of [44]. An additional adjustment of the hole energies has been done to reproduce the experimental position of the IAS. (It is well known that the IAS energy obtained in the RPA approaches is about of 1 MeV lower than the experimental one. The problem can be solved adequately in a fully self-consistent framework and provided the Coulomb correlation energy is properly accounted for [39, 130].) The procedure of the adjustment of the hole energies to reproduce the IAS position [158] leads to the A-dependent renormalization of the Landau–Migdal strength parameter g_0' [121]. Together with the non-self-consistent treatment of the single-particle energies, this influences the GT strength function and calculated (ν_e, e^-) rates, especially for the neutrino spectra with high average energies. Thus, the calculations of the giant GT resonances based on the self-consistent treatment of the ground-state properties are especially important for unstable neutron-rich nuclei. Table 2 contains the GT centroid energies for tin isotopes calculated within the ETFSI + CQRPA [121] (the value of the g' constant of the Landau–Migdal interaction Eq. (34) was fixed to describe the position of the GTR in ^{208}Pb, and has remained unchanged for other A).

Table 2. **Experimental** (p, n) **reaction** Q **values** Q_{pn} **and GTR maximum energies** $E_x = Q_{pn} - \omega_{pn}$ **in the tin isotopes chain in comparison with the ones calculated using the SkSC17 Skyrme interaction [121]**

Nucleus	$-Q_{pn}$, MeV		E_x, MeV	
	SkSC17	Exp. [162]	SkSC17	Exp. [162]
^{112}Sn	7.30	7.06	8.6	8.94(25)
^{114}Sn	6.07	5.88	9.3	9.39(25)
^{116}Sn	4.55	4.71	10.2	10.04(25)
^{117}Sn	1.77	1.76	12.6	12.87(25)
^{118}Sn	3.52	3.66	10.5	10.61(25)
^{119}Sn	0.71	0.59	13.2	13.71(25)
^{120}Sn	2.50	2.68	11.0	11.45(25)
^{122}Sn	1.53	1.62	12.1	12.25(25)
^{124}Sn	1.00	0.62	13.0	13.25(25)

In general, the results of [158] with low neutrino temperatures $T_\nu \leq 4$ MeV are close to the ones obtained in [121]. For these temperatures a momentum dependence of the transition operators reduces the cross sections roughly by 20 %, while taking into account the FF contribution increases the cross sections by about 25–50 % [158]. Thus, for these temperatures ($\bar{E}_\nu \lesssim 12$ Mev), the contribution of the IAS and GT excitations mostly define the total cross section of the charged-current neutrino capture. (This is in agreement with the Skyrme-RPA calculations [163], the results of which show that FF transitions do not give a significant contribution to the $^{208}\mathrm{Pb}(\nu_e, e^-)$ for $\bar{E}_\nu \leq 15$ MeV.) In the neutrino oscillation scenario, the situation changes; as for the high neutrino temperatures $T_\nu \gtrsim 8$ MeV, the average neutrino energies $\bar{E}_\nu \gtrsim 25$ MeV allow the excitation of the spin-dipole $\Delta L = 1$ resonances which increase the cross sections by a factor up to 3 [158].

It is of importance that the total $(\nu_e - A)$ cross sections for both calculations [121, 158] decrease almost linearly with the increasing charge number Z (Fig. 15). This dependence is natural, first, because the shifts of the IAS and GTR centroids down in energy (relative to the parent ground state) are roughly proportional to Z. At the same time, the total strengths for the IAS and GT resonances (dominating the total cross section) are bound by the model-independent sum rules which are proportional to $\sim (N - Z)$. Therefore, both the corresponding half-lives against the (ν_e, e^-) capture at $N = 50$, 82, 126 and β-decay half-lives increase approaching the closed $Z = 28$, 50, 82 shells.

Now, let us turn again to Fig. 13 where we show together with the half-lives of the nuclei at $N = 126$ also the calculated half-lives against the (ν_e, e^-) capture. In the specific case of the neutrino wind model, the charged-current electron neutrino captures by heavy nuclei — (ν_e, e^-) compete with the β decays in driving the material to higher Z elements. Thus, the effective «weak flow» rate is given by $\lambda_{\mathrm{eff}} = \lambda_\beta + \lambda_\nu$. The neutrino capture rates are however sensitive to the adopted neutrino driven wind model, since they depend on the neutrino flux which scales with the R^2 — the distance to the centre of the neutron star. The (ν_e, e^-)-capture rates would also increase if the neutrino oscillations $\nu_e \rightleftharpoons \nu_{\mu,\tau}$ are included.

In Fig. 13, the (ν_e, e^-)-capture «half-lives» are shown corrected for the contribution of the forbidden transitions at the electron neutrino temperature $T_\nu = 4$ MeV [121], and the calculations by [158] at $T_\nu = 8$ MeV in which the complete neutrino conversion $\nu_{\mu,\tau} \rightleftharpoons \nu_e$ was assumed. As is seen in Fig. 13, even at $T_\nu = 8$ MeV the β-decay rates calculated with inclusion of the FF transitions are significantly larger than the corresponding (ν_e, e^-) rates for nuclides with $Z \leq 69$. In other words, for these given temperatures and neutrino flux, β decays dominate over charged-current electron neutrino captures. The possible implications on the r-process nucleosynthesis in the $N = 126$ region which may arise due to the shorter β-decay half-lives should be discussed in terms of the specific r-process model.

The charge-current (CC) neutrino capture and neutral-current (NC) inelastic neutrino scattering can also give rise to neutrino-induced nucleon spallation. As the excitation energy of a daughter nucleus in the charge-current neutrino reactions may well exceed the Q_β value, allowing the excitation, the excitation of their GT and spin-dipole $\Delta L = 1$ resonances above the neutron thresholds is possible followed by multiple neutron emission. For instance, the average number of emitted neutrons of 6.2 to 2.3 has been estimated in [158] for the $(\nu_e, e^- k(n))$ reaction ($T_\nu = 4$ MeV, $\alpha = 0$) on the $N = 126$ and $Z = 65{-}76$ nuclei. For the neutral-current ν_x, ν'_x reactions due to the high average energy of the heavy-flavor neutrino ($\bar{E}_{\nu_x} \approx 25$ MeV in the case without oscillations), the excitation of the non-charge-exchange giant resonances in the continuum causes multiple proton and neutron emissions. The estimated average number of emitted neutrons is of 3.2 to 1.5 for the (ν_e, e^-) reaction ($T_\nu = 8$ MeV, $\alpha = 0$) on the $N = 126$, $Z = 65{-}76$ nuclei [158].

Due to the high Z and specific spectral properties, the heavy nuclei like ^{54}Fe and ^{208}Pb may serve as efficient neutrino-to-neutron «converters». This gives a possibility of a high statistic detection of the supernova neutrinos and observation of their oscillation signatures in the terrestrial neutron spallation laboratories, such as recently proposed *Observatory for Multiflavor Neutrinos from Supernovae* (OMNIS) and *Lead Astronomical Neutrino Detector* (LAND). The detectors register the signals of the one- and two-neutron emission which follow the NC neutrino excitation or/and CC neutrino dissociation of the ^{54}Fe and ^{208}Pb. The (ν, n) threshold for NC scattering on ^{208}Pb is quite low (7.37 MeV), and the one for CC dissociation of ^{208}Bi is only 9.77 MeV. The higher-energy neutrinos may also cause the two-neutron emission from ^{208}Pb with the threshold of 14.98 MeV. According to the estimate by [164], a supernova at a distance of 8 kpc produce about 780 neutrons per kT of lead for neutrinos of all flavors (assuming the standard ν spectra given by Eq. (37)). The yield of the CC events from ^{208}Bi is expected to be only 47 events/per kT, but the two-neutron emission rate of ^{208}Bi is shown to be flavor specific and sensitive to the mean neutrino energy (ν temperature). With complete $\nu_x \rightleftharpoons \nu_e$ oscillations in effect, the gross-theory-based estimate predicts the increase of the channel-integrated two-neutron signal in ^{208}Pb by a factor of about 40 [164]. By contrast, the NC (ν, n) threshold in iron is rather high (11.20 MeV), and the rate of the CC processes is negligibly small. Though, the production efficiency for iron is lower (140 neutron/per kT), a yield should be independent of the ν oscillation. Thus, both the ratio of the one- to two-neutron signals in lead, and the one of the lead to iron signals are sensitive to the extent of the $\nu_x \rightleftharpoons \nu_e$ oscillations.

However, for high mean neutrino energy, the simplified estimate by [164] should be verified by the consistent microscopic calculations. In this case, in addition to IAS and GT, the important contribution comes from the $\Delta L = 1$ spin-dipole charge-exchange resonances in continuum for which the empirical

energy systematics used in [164] cannot be considered as a reliable one. Making use of the «full» experimental strength function including the «tail» in continuum region would be safer. In the (p, n) experiments [165] the energy splitting of the $S = 0$ and $S = 1$ components of the $J^\pi = 1^-$ resonance in ^{208}Pb has been found to be 4.7 ± 2 MeV, however the experimental uncertainty is still high to extract a reliable strength function which can be used to estimate the σ_{ν_e}.

The microscopic calculations of the $^{208}\mathrm{Pb}(\nu_e, e^-)$ cross section have been performed in [163, 166]. Their results also deviate from each other, in particular because the strength functions of the $S = 0$ and $S = 1$ multipole charge-exchange resonances are sensitive to the adopted spin-independent and spin-dependent NN interactions and especially to their density-dependence [130]. Thus, the flux-averaged $^{208}\mathrm{Pb}(\nu_e, e^-)$ cross sections at ($\alpha = 0$, $T = 6$ MeV) calculated within the WS-RPA [166] are lower by a factor of 2.5 than the ones from [164]. At the same time, the result of the self-consistent Skyrme-RPA calculations [163] which account for the «FF transitions» with the multipolarities $J \lesssim 7$ is lower than the gross-theory estimate by a factor of 2.

To summarize Sec. 2, one has to admit that, although the astrophysical environments in which the r process takes place remain to be elucidated, a reliable prediction of the r-process elemental abundances requires an accurate knowledge of the β-decay rates and the (ν_e, e^-) rates for few thousands nuclei of relevance. As has been shown in Sec. 2, in predicting the nuclear weak rates for the r-process modeling one faces two specific features of the problem: a nonstatistical origin of the β-strength function, and the need to consider a huge number of very neutron-rich nuclei which are experimentally unknown. For these reasons, the performance of the CQRPA approach based on the self-consistent ground state description is already better than of the phenomenological and simplified semi-microscopic models. For example, the DF + CQRPA calculations [125,126] which treat the GT and FF decays on the same footing provide more accurate description of the recent experimental β half-lives of the short-lived neutron-rich nuclei. A possibility to reliably estimate the (ν_e, e^-) cross section in the stable nucleus ^{208}Pb has been demonstrated by the self-consistent Skyrme-RPA calculation [163]. At the same time, there is a strong need for fully self-consistent predictions of the weak rates and of spin-isospin response in continuum. The accelerator based β-decay experiments [142–145] and $\nu_{e,\mu}$-capture experiments [167, 168] are of great importance, as they put rigid constraints on the theoretical models.

CONCLUSIONS

An important effort has been devoted in the last decades to measure the decay half-lives and reaction cross sections relevant for astrophysics. However, major difficulties related to the specific conditions of the astrophysical plasma remain

(charged-particle capture at low energies, large number of nuclei and properties to consider, nuclei far from stability under extreme conditions: high-temperature and/or high-density environments, ...). In many astrophysical scenarios, the nuclear data of need have to be predicted exclusively by theoretical modeling.

The extrapolation to exotic nuclei or energy ranges far away from experimentally known regions constrains the use of nuclear models to the most reliable ones. Both phenomenological and microscopic approaches have to be further improved. In a first approximation, microscopic approaches can benefit from using phenomenological ingredients. However, even if purely phenomenological description presents a better ability to reproduce experimental data, more attention should be paid to developing approaches relying on the self-consistent treatment of the ground-state properties and on the universal ansatzs for the nuclear energy-density functional or corresponding effective NN interaction. This way, a kind of compromise between the reliability, accuracy and applicability of the different theories available has to be found according to the specific application considered. In addition, further investigations should aim at describing reliably and possibly accurately all nuclear properties within one unique framework. This universality aspect of the microscopic predictions corresponds to one of the major challenges of fundamental nuclear physics research for the coming decades.

Due to impressive progress in computational capabilities, microscopic models can now be adjusted to reach a level of accuracy similar to (or better than) the phenomenological models. For specific practical applications they can be renormalized on experimental data if needed, and replace the phenomenological approaches little by little in practical applications. A continued efforts to improve our predictions of the reaction and β-decay rates relevant to astrophysics are obviously required. Those include a better description of the ground-state properties (and most particularly an improved treatment of the nuclear pairing force), nuclear level density and the α-nucleus optical potential, as well as a better understanding of given nuclear effects affecting exotic neutron-rich nuclei, such as the soft dipole modes. The description of the direct capture contribution also remains to be based on extended nuclear models. In this case, the spectroscopic properties below the neutron separation energy need to be estimated. Developing fully self-consistent models for the description of β-decay properties of spherical and deformed nuclei is an important challenge. This continued effort to improve and extend the microscopic nuclear predictions is concomitant with new measurements of masses and β-decay half-lives far away from stability, and also of relevant reaction cross sections on stable and unstable targets.

Acknowledgments. One of the authors (I. B.) is grateful to the FNRS for the support within the IISN Programme, S. G. is FNRS senior research assistant. It is our pleasure to thank Profs. M. Arnould and J. M. Pearson for continuous interest in this work. I. B. is grateful to Profs. P. Ring and E. Roeckl for stimulating discussions, to S. V. Tolokonnikov for valuable advises and to the participants of

the Programme IAP P5/07 «Exotic Nuclei for Nuclear Physics and Astrophysics» at the IKS, Leuven for fruitful collaboration.

REFERENCES

1. *Arnould M. et al.* Impact and applications of nuclear science in Europe. NuPECC Report / Ed. A. van der Woude. 1994. P. 157.
2. *Arnould M., Takahashi K.* Nuclear astrophysics // Prog. Part. Nucl. Phys. 1999. V. 62. P. 393–463.
3. *Arnould M., Goriely S., Jorissen A.* Non-explosive hydrogen and helium burnings: abundance predictions from the NACRE reaction rate compilation // Astron. Astrophys. 1999. V. 347. P. 57.
4. *Hoffman R. D. et al.* The reaction rate sensitivity of nucleosynthesis in type II supernovae // Astrophys. J. 1999. V. 521. P. 735.
5. *Käppeler F., Beer H., Wisshak K.* s-process nucleosynthesis: nuclear physics and the classical model // Prog. Part. Nucl. Phys. 1989. V. 52. P. 945–1013.
6. *Goriely S.* Uncertainties in the solar system r-abundance distribution // Astron. Astrophys. 1999. V. 342. P. 881.
7. *Goriely S., Mowlavi N.* Neutron-capture nucleosynthesis in AGB stars // Astron. Astrophys. 2000. V. 362. P. 599–614.
8. *Goriely S., Arnould M.* Waiting point approximation and canonical multi-event r-process revisited // Astron. Astrophys. 1996. V. 312. P. 327.
9. *Goriely S.* Direct neutron captures and the r-process nucleosynthesis // Astron. Astrophys. 1997. V. 325. P. 414.
10. *Goriely S.* Nuclear masses and the r- and p-processes of nucleosynthesis // Hyp. Int. 2001. V. 132. P. 105.
11. *Arnould M., Takahashi K.* Astrophysical ages and dating methods. Editions Frontières / Eds. E. Vangioni-Flam et al. 1990. P. 325.
12. *Goriely S., Clerbaux C.* Uncertainties in the Th cosmochronometry // Astron. Astrophys. 1999. V. 346. P. 798.
13. *Bosch F. et al.* Observation of bound-state β^--decay of fully ionized ^{187}Re: ^{187}Re–^{187}Os cosmochronometry // Phys. Rev. Lett. 1996. V. 77. P. 5190.
14. *Arnould M., Goriely S.* The p-process of stellar nucleosynthesis: Astrophysics and nuclear physics status // Phys. Rep. 2003 (submitted).
15. *Rayet M. et al.* The p-process in type II supernovae // Astron. Astrophys. 1995. V. 298. P. 517.
16. *Costa V. et al.* The synthesis of the light Mo–Ru isotopes: how now, no need for an exotic solution? // Astron. Astrophys. 2000. V. 358. P. L67.
17. *Hauser W., Feshbach H.* // Phys. Rev. 1952. V. 87. P. 366.
18. *Holmes J. A. et al.* Tables of thermonuclear-reaction-rate data for neutron-induced reactions on heavy nuclei // At. Data Nucl. Data Tables. 2000. V. 18. P. 306–412.
19. *Mathews G. J. et al.* Neutron capture rates in the r-process: the role of direct radiative capture // Astrophys. J. 1983. V. 270. P. 740–745.
20. *Jeukenne J. P., Lejeune A., Mahaux C.* Optical-model potential in finite nuclei, from Reid's hard core interaction // Phys. Rev. C. 1977. V. 16. P. 80–96.

21. *Cerf N.* Realistic microscopic level densities for spherical nuclei // Phys. Rev. C. 1994. V. 50. P. 836–844.

22. *Audi G., Wapstra A. H.* The 1995 update to the atomic mass evaluation // Nucl. Phys. A. 1995. V. 595. P. 409–480.

23. *Audi G., Wapstra A. H.* Private communication. 2002.

24. *von Weizsäcker C. F.* // Zeit. Phys. A. 1935. V. 99. P. 431.

25. *Myers W. D., Swiatecki W. J.* Nuclear masses and deformations // Nucl. Phys. 1966. V. 81. P. 1–60.

26. *Möller P. et al.* Nuclear ground-state masses and deformations // At. Data Nucl. Data Tables. 1995. V. 59. P. 185–381.

27. *Aboussir Y. et al.* Nuclear masses via an approximation to the Hartree–Fock method // Ibid. V. 61. P. 127–176.

28. *Goriely S.* Capture gamma-ray spectroscopy and related topics. AIP / Ed. S. Wender. 2000. P. 287.

29. *Tondeur F. et al.* Towards a Hartree–Fock mass formula // Phys. Rev. C. 2000. V. 62. P. 024308.

30. *Goriely S., Tondeur F., Pearson J.M.* A Hartree–Fock nuclear mass table // At. Data Nucl. Data Tables. 2000. V. 77. P. 311–381.

31. *Samyn M. et al.* A HFB mass formula // Nucl. Phys. A. 2002. V. 700. P. 142.

32. *Goriely S. et al.* Hartree–Fock mass formulas and extrapolation to new mass data // Phys. Rev. C. 2002. V. 66. P. 024326.

33. *Bohigas O., Leboeuf P.* Nuclear masses: evidence of order-chaos coexistence // Phys. Rev. Lett. 2002. V. 88. P. 092502-1-5.

34. *Farine M., Pearson J. M., Tondeur F.* Skyrme force with surface-peaked effective mass // Nucl. Phys. A. 2002. V. 696. P. 396.

35. *Ring P.* Relativistic mean field theory // Prog. Part. Nucl. Phys. 1996. V. 37. P. 193–241.

36. *Khodel V. A., Saperstein E. E.* Quasiparticle Lagrangian approach to atomic nuclei // Phys. Rep. 1982. V. 92. P. 183–224.

37. *Khodel V. A., Saperstein E. E., Zverev M. V.* // Nucl. Phys. A. 1987. V. 465. P. 397.

38. *Fayans S. A., Khodel V. A.* Self-consistency relations in finite Fermi systems // JETP Lett. 1973. V. 16. P. 633.

39. *Smirnov A. V., Tolokonnikov S. V., Fayans S. A.* The local energy density functional in atomic nuclei // Sov. J. Nucl. Phys. A. 1984. V. 48. P. 995–1003;
Fayans S. A. et al. Nuclear isotope shifts within the local energy-density functional approach // Nucl. Phys. A. 2000. V. 676. P. 49–119.

40. *Hohenberg A., Kohn W.* Inhomogeneous electron gas // Phys. Rev. C. 1964. V. 136. P. B864–B871.

41. *Fayans S. A.* Towards a universal nuclear density functional // JETP Lett. 1998. V. 68. P. 169–174.

42. *Fridman B., Panharipande V. R.* Equation of state of neutron matter // Nucl. Phys. A. 1981. V. 361. P. 501–523.

43. *Wiringa R. B., Fiks V., Fabrocini A.* Equation of state of nuclear matter // Phys. Rev. C. 1988. V. 38. P. 1010–1028.

44. *Duflo J., Zuker A.* Microscopic nuclear mass models // Phys. Rev. C. 1995. V. 52. P. R23–R27.

45. *Otsuka T. et al.* Magic numbers in exotic nuclei and spin-isospin properties of the NN interaction // Phys. Rev. Lett. 2001. V. 87. P. 082502.

46. *Ignatyuk A. V.* Statistical properties of excited atomic nuclei. IAEA-INDC(CCP)-233/L. 1985. P. 1–119.

47. Reference Input Parameter Library. IAEA-Tecdoc-1034. 1998 (also available at http://iaeand.iaea.or.at/ripl).

48. *Goriely S.* A new nuclear level density formula including shell and pairing correction in the light of a microscopic model calculation // Nucl. Phys. A. 1996. V. 605. P. 28–60.

49. *Goriely S.* Nuclear reaction data relevant to nuclear astrophysics // J. Nucl. Scien. Techn. 2002. No. 2. P. 536–541.

50. *Decowski P. et al.* On superconductivity effects in nuclear level density // Nucl. Phys. A. 1968. V. 110. P. 129–141.

51. *Moretto L.G.* Statistical description of a paired nucleus with the inclusion of angular momentum // Nucl. Phys. A. 1972. V. 185. P. 145–165.

52. *Demetriou P., Goriely S.* Microscopic nuclear level densities for practical applications // Nucl. Phys. A. 2001. V. 695. P. 95–108.

53. *Hilaire S., Delaroche J. P., Koning A. J.* Generalized particle-hole state densities within the equidistant spacing model // Nucl. Phys. A. 1998. V. 632. P. 417–441.

54. *Siem S. et al.* Level densities and gamma-strength functions in ^{148,149}Sm // Phys. Rev. C. 2002. V. 65. P. 044318.

55. *Bauge E., Delaroche J. P., Girod M.* Semimicroscopic nucleon-nucleus spherical optical potential model for nuclei with $A \geq 40$ at energies up to 200 MeV // Phys. Rev. C. 1998. V. 58. P. 1118.

56. *Bauge E., Delaroche J. P., Girod M.* Lane-consistent, semimicroscopic nucleon–nucleus optical model // Phys. Rev. C. 2001. V. 63. P. 024607.

57. *Zuo W., Bombaci I., Lombardo U.* Asymmetric nuclear matter from an extended Brueckner–Hartree–Fock approach // Phys. Rev. C. 1999. V. 60. P. 024605.

58. *Mc Fadden L., Satchler G. R.* // Nucl. Phys. A. 1966. V. 84. P. 177.

59. *Somorjai E. et al.* Experimental cross section of ^{144}Sm$(\alpha,\gamma)^{148}$Gd and implications for the p-process // Astron. Astrophys. 1998. V. 333. P. 1112–1116.

60. *Grama C., Goriely S.* Nuclei in the cosmos. Editions Frontières / Eds. N. Prantzos et al. 1998. P. 463.

61. *Mohr P.* α-nucleus potentials for the neutron-deficient p nuclei // Phys. Rev. C. 2000. V. 61. P. 045802.

62. *Demetriou P., Grama C., Goriely S.* Improved global alpha-optical model potentials at low energies // Nucl. Phys. A. 2002. V. 707. P. 142–156.

63. *Kobos A.M. et al.* Folding-model analysis of elastic and inelastic α-particle scattering using a density-dependent force // Nucl. Phys. A. 1984. V. 425. P. 205.

64. *Kopecky J., Chrien R.E.* Observation of the $M1$ giant resonance by resonance averaging in ^{106}Pd // Nucl. Phys. A. 1987. V. 468. P. 285–300.

65. *Kopecky J., Uhl M.* Test of gamma-ray strength functions in nuclear reaction model calculations // Phys. Rev. C. 1990. V. 41. P. 1941–1955.

66. *Goriely S.* Radiative neutron captures by neutron-rich nuclei and the r-process nucleosynthesis // Phys. Lett. B. 1998. V. 436. P. 10–18.

67. *Kadmenskii S. G., Markushev V. P., Furman V. I.* Radiative widths of neutron resonances. Giant dipole resonances // Sov. J. Nucl. Phys. 1983. V. 37. P. 165–168.

68. *Govaert K. et al.* Dipole excitations to bound states in ^{116}Sn and ^{124}Sn // Phys. Rev. C. 1998. V. 57. P. 2229–2249.

69. *Myers W. D. et al.* Droplet model of the giant dipole resonance // Phys. Rev. C. 1977. V. 15. P. 2032–2043.

70. *Goriely S., Khan E.* Large-scale QRPA calculation of $E1$ strengths and its impact on the neutron capture cross section // Nucl. Phys. A. 2002. V. 706. P. 217–232.

71. Photonuclear data for applications; cross sections and spectra. IAEA-Tecdoc-1178. 2000.

72. *Colo G., Bortignon P. F.* QRPA plus phonon coupling model and the photoabsorbtion cross section for ^{18,20,22}O // Nucl. Phys. A. 2001. V. 696. P. 427–441.

73. *Langanke K., Martinez-Pinedo G.* Nuclear weak-interaction processes in stars // Rev. Mod. Phys. 2002 (in print); nucl-th/0203071. 2002.

74. *Burbidge E. M. et al.* // Rev. Mod. Phys. 1957. V. 29. P. 547–599.

75. *Woosley S. E., Hoffman R.* The α-process and the r-process // Astrophys. J. 1992. V. 395. P. 202–239.

76. *Woosley S. E. et al.* The r-process and neutrino-heated supernova ejecta // Astrophys. J. 1994. V. 433. P. 229–246.

77. *Witti J., Janka T.-H., Takahashi K.* I. The α-process // Astron. Astrophys. 1994. V. 286. P. 841–856;
Takahashi K., Witti J., Janka H. T. Nucleosynthesis in neutrino-driven winds from protoneutron stars (II. The r-process) // Ibid. P. 857–869.

78. *Truran J., Cowan J. J., Fields B. D.* Halo star abundances and r-process synthesis // Nucl. Phys. A. 2000. V. 488. P. 330c–339c.

79. *Rosswog S., Freiburghaus C., Thielemann F.-K.* Nucleosynthesis calculations for ejecta of neutron star coalescences // Nucl. Phys. A. 2001. V. 688. P. 344c–348c.

80. *McLaughlin G., Fuller G. M.* Neutrino capture by heavy nuclei // Astrophys. J. 1995. V. 455. P. 202–214.

81. *Zyryanova L. N.* Unique beta transitions (Russ. original: M.; L.: Acad. Science USSR, 1960; Once forbidden beta transitions (translation: Pergamon Press, 1963).

82. *Gove N. B., Martin M. J.* Log-f tables for beta decay // At. Data Nucl. Data Tables. 1971. V. 10. P. 206–317.

83. *Cameron E.* // Ann. Rev. Nucl. Sci. 1958. V. 8. P. 299–364.

84. *Izosimov I. N.* Manifestations of non-statistical effects in nuclei // Phys. Part. Nucl. 1999. V. 30, No. 2. P. 131–155.

85. *Takahashi K., Yamada M., Kondoh T.* Beta-decay half-lives calculated on the gross-theory // At. Data Nucl. Data Tables. 1975. V. 12. P. 101–142.

86. *Tachibana T., Yamada M., Yoshida N.* An improvement of the gross-theory of β decay // Prog. Theor. Phys. 1992. V. 84. P. 641–111.

87. *Nakata H., Tachibana T., Yamada M.* Semi-gross theory of the β decay // Nucl. Phys. A. 1997. V. 625. P. 521–111.

88. *Martinez-Pinedo G., Langanke K.* Shell-model half-lives for the $N = 82$ nuclei and their implications for the r-process // Phys. Rev. Lett. 1999. V. 83. P. 4502–4505.

89. *Martinez-Pinedo G.* Weak interaction rates in astrophysics // Nucl. Phys. A. 2000. V. 668. P. 357c–363c.

90. *Caurier E. et al. Ab initio* shell model for $A = 10$ nuclei // Phys. Rev. C. 2002. V. 66. P. 024314-1-14.

91. *Warburton E. K.* First-forbidden β decay in the lead region and mesonic enhancement of weak axial current // Phys. Rev. C. 1991. V. 44. P. 233–260.

92. *Michel N. et al.* First-forbidden mirror β decays in $A = 17$ region // Nucl. Phys. A. 2002. V. 703. P. 202–221.

93. *Dukelsky J. et al.* Density matrix renormalization group method and large-scale shell model calculations // Phys. Rev. 2002. V. 65. P. 054319-1-8.

94. *Zamic L. et al.* Towards self-consistent shell-model // Ibid. P. 054321-1-8.

95. *Towner I. S., Warburton E. K., Garvey G. T.* Hindrance phenomena in unique first- and third-forbidden β decay // Ann. Phys. 1971. V. 66. P. 674–696.

96. *Alexankin V. G., Lutostanskii Yu. S., Panov I. V.* Half-lives of nuclei far from stabilty line, and the structure of the β-decay strength function // Sov. J. Nucl. Phys. A. 1985. V. 34. P. 804–809; *Gaponov Yu. V., Lutostansky Yu. S.* Microscopic description of the Gamow–Teller resonance and collective isobaric states in spherical nuclei // Sov. J. Part. Nucl. A. 1981. V. 12. P. 528–545.

97. *Migdal A. B.* Theory of finite Fermi systems and applications to atomic nuclei (translation of the 1st Russian ed. N. Y.: Interscience, 1967).

98. *Krumlinde J., Möller P.* Calculation of Gamow–Teller β-strength functions in the Rb region in the RPA approximation with Nilsson-model wave functions // Nucl. Phys. A. 1984. V. 417. P. 419–446;
Möller P., Rundrup J. New developments in the calculation of β-strength functions // Nucl. Phys. A. 1990. V. 514. P. 1–48.

99. *Möller P., Nix J. R., Kratz K.-L.* Tables of beta decay characteristics for astrophysical and radioactive beam applications // At. Data Nucl. Data Tables. 1997. V. 66. P. 131–211.

100. *Audi G. et al.* The Nubase evaluation of nuclear and decay properties // Nucl. Phys. A. 1997. V. 624. P. 1–124.

101. *Engel J., Vogel P., Zirnbauer M. R.* Nuclear structure effects in double-beta decay // Phys. Rev. C. 1988. V. 37. P. 731–746.

102. *Suhonen J., Tagiel T., Faessler A.* pnQRPA calculation of the β^+/EC quenching for several neutron-deficient nuclei in mass regions $A = 94-110$ and $A = 146-156$ // Nucl. Phys. A. 1988. V. 486. P. 91–117.

103. *Borzov I. N., Trykov E. L.* Microscopic analysis of the non-equilibrium component of charge-exchange spectra // Sov. J. Nucl. Phys. A. 1990. V. 52. P. 52–63;
Borzov I. N., Trykov E. L., Fayans S. A. Strength functions of Gamow–Teller excitations of stable and neutron-deficient nuclei // Ibid. P. 627–637.

104. *Moller P., Pfeifer B., Kratz K.-L.* New calculations of gross β-decay properties for astrophysical applications. LANL-Preprint-UR-02-2919. 2002.

105. *Staudt A. et al.* Second generation microscopic predictions of β-decay half-lives of neutron-rich nuclei // At. Data Nucl. Data Tables. 1990. V. 44. P. 79–132;
Hirsch M., Staudt A., Klapdor-Kleingrothaus H.-V. Prediction of average β and γ energies and probabilities of β-delayed neutron emission in the region of fission products // At. Data Nucl. Data Tables. 1992. V. 51. P. 244–244.

106. *Birbrair B. L.* Density matrix approach to the atomic nuclei // Nucl. Phys. A. 1968. V. 108. P. 449–477.

107. *Nabi J.-U., Klapdor-Kleingrothaus H.-V.* Weak interaction rates of sd-nuclei in stellar environments calculated inthe pn approximation // At. Data Nucl. Data Tables. 1999. V. 71. P. 149–346.

108. *Homma H. et al.* Systematic study of nuclear β decay // Phys. Rev. C. 1996. V. 54. P. 2972–2985.

109. *Soloviev V. G.* Theory of atomic nuclei: quasiparticles and phonons. Bristol: Institute of Physics Publishing, 1992.

110. *Kuzmin V. A., Soloviev V. G.* Gamow–Teller β^+ decays and strength functions of (n, p) transitions in spherical nuclei // Nucl. Phys. A. 1988. V. 486. P. 118–132.

111. *Giai N. V., Stoyanov Ch., Voronov V. V.* Finite rank approximation for RPA calculations with Skyrme interactions: an application to Ar isotopes // Phys. Rev. C. 1999. V. 57. P. 1204–1209; *Severyukhin A. P. et al.* QRPA with finite rank approximation for Skyrme interactions // Phys. Rev. C. 2002. V. 66. P. 034304-1-7.

112. *Borzov I. N., Fayans S. A., Trykov E. L.* Gamow–Teller strength functions of superfluid odd-A nuclei and neutrino capture reactions // Nucl. Phys. A. 1995. V. 584. P. 335–361.

113. *Borzov I. N. et al.* Ground state properties and β-decay half-lives near ^{132}Sn in a self-consistent theory // Zeit. Phys. A. 1996. V. 355. P. 117–127.

114. *Migdal A. B.* Theory of finite Fermi systems and atomic nuclei properties (Russ. original 2nd ed. M.: Nauka, 1983).

115. *Platonov A. P., Saperstein E. E.* Response functions of superfluid nuclei and low-lying quadrupole vibrations // Nucl. Phys. A. 1988. V. 486. P. 63–76.

116. *Borzov I. N. et al.* Pionic degrees of freedom and effects of nuclei near the point of pion condensation // Sov. J. Part. Nucl. A. 1981. V. 12. P. 848–904.

117. *Borzov I. N., Tolokonnikov S. V., Fayans S. A.* Spin-dependent effective nucleon-nucleon interaction in nuclei // Sov. J. Nucl. Phys. A. 1984. V. 40(5). P. 732–739.

118. *Gaarde C.* Spin-isospin excitations in nuclei // Nucl. Phys. A. 1983. V. 396. P. 127c–134c.

119. *Wakasa T. et al.* Gamow–Teller strength of ^{90}Nb in the continuum studied via multiple decomposition analysis of the ^{90}Zr(p, n) reaction at 295 MeV // Phys. Rev. C. 1999. V. 55. P. 2909–2922;
Sakai H., Gamow–Teller strength and quenching: probed by recent precise (p, n) and (n, p) measurements at 300 MeV // Nucl. Phys. A. 2000. V. 690. P. 66c–77c.

120. *Borzov I. N., Goriely S., Pearson J. M.* Microscopic calculations of β-decay characteristics near the $A = 130$ r-process peak // Nucl. Phys. A. 1997. V. 621. P. 307c–311c; and www-astro.ulb.ac.be

121. *Borzov I. N., Goriely S.* Weak interaction rates and the r-process nucleosynthesis // Phys. Rev. C. 2000. V. 62. P. 035501–035512.

122. *Borzov I. N.* // Proc. of Intern. Workshop «Beta decay: from weak interaction to nuclear structure», Strasbourg, 1999. P. 73.
Borzov I. N. Electron neutrino capture rates for astrophysical applications // Nucl. Phys. A. 2001. V. 668. P. 382c–385c.

123. *Goriely S. et al.* The puzzle of the synthesis of the rare nuclide ^{138}La // Astron. Astrophys. 2001. V. 375. P. 35L–39L.

124. *Kubodera T., Delorme J., Rho M.* Axial currents in nuclei // Phys. Lett. B. 1982. V. 45. P. 755–758.

125. *Borzov I. N.* Hartee–Fock-BCS calculations of the beta-decay half-lives // Proc. of the NATO Advanced Research Workshop on Nuclear Many Body Problem, Brijuni, Pula, Croatia, 2001. Kluwer Academic Publishers, 2002. P. 323–328.

126. *Borzov I. N.* Gamow–Teller and first-forbidden decays near the r-process paths at $N = 50$, 82, 126. PRC20036828502-1-14.

127. *Engel J. et al.* β-decay rates of r-process waiting-point nuclei in the self-consistent approach // Phys. Rev. C. 1999. V. 60. P. 014302-1-11.

128. *Bender M. et al.* Gamow–Teller strength and the spin-isospin coupling constants of the Skyrme energy functional // Phys. Rev. C. 2002. V. 65. P. 054322-1-21.

129. *Blomquist J., Kerek M., Fogelberg B.* The single proton nucleus ^{133}Sb // Zeit. Phys. A. 1983. V. 314. P. 199–204;
Korgul A. et al. Structure information on the r-process nucleus ^{135}Sn // Phys. Rev. 2001. V. 63. P. 021302-1-5.

130. *Pyatov N. I., Fayans S. A.* Change-exchange excitations of nuclei // Sov. J. Part. Nucl. A. 1983. V. 14. P. 401–464.

131. *Matsuo M.* Continuum linear response in coordinate space HFB formalism for collective excitations in drip-line nuclei // Nucl. Phys. A. 2001. V. 696. P. 371–395.

132. *Khan E. et al.* Continuum quasiparticle random phase-approximation and the time-dependent Hartree–Fock–Bogolubov approach // Phys. Rev. C. 2002. V. 66. P. 024309-1-14.

133. *Paar N. et al.* QRPA based on the relativistic HFB model. Preprint nucl-th-0212011v2. 2002. P. 1–21.

134. *Bulgac A.* HFB approximation for finite systems. Preprint-CIP-INPE 1980. P.1–15.

135. *Bulgac A.* Local density approximation for systems with pairing correlations // Phys. Rev. 2002. V. 65. P. R051305-1-4.

136. *Delion D. S., Santos S., Shuck P.* Pairing effect in delayed neutron emission // Phys. Lett. B. 1997. V. 398. P. 1–5.

137. *Baldo M. et al.* Existence of nuclei with unusual neutron excess? // Phys. Lett. B. 2002. V. 533. P. 17–21.

138. *Dobaczewski J. et al.* Nuclear shell structure at particle drip-lines // Phys. Rev. Lett. 1994. V. 72. P. 981–984.

139. *Franchoo S. et al.* Beta-decay of $^{68-74}$Ni and level structure of neutron-rich Cu isotopes // Phys. Rev. Lett. 1998. V. 81. P. 3100–2103.

140. *Fedoseev V. N. et al.* Study of short-lived silver isotopes with laser ion source // Zeit. Phys. A. 1995. V. 353. P. 9–10.

141. *Hannawald M. et al.* Selective laser ionization of very neutron-rich cadmium isotopes: decay properties of ^{131}Cd and ^{132}Cd // Phys. Rev. C. 2000. V. 62. P. 054301-1-9.

142. *Shergur J. et al.* β-decay studies of $^{135-137}$Sn using selective laser ionization techniques // Phys. Rev. C. 2002. V. 65. P. 034313-1-12.

143. *Kurpeta J. et al.* The decay of the neutron-rich nucleus ^{216}Bi // Eur. J. Phys. A. 2000. V. 7. P. 49–54.

144. *DeWitte H. et al.* First observation of the β decay of neutron-rich ^{218}Bi by the pulsed-release technique and resonant laser ionization // Eur. J. Phys. 2003 (in print).

145. *Kratz K.-L.* Measurements of r-process nuclei // Nucl. Phys. A. 2000. V. 668. P. 308c–317c.

146. *Vetterli M. C. et al.* Gamow–Teller strength deduced from charge-exchange reactions on ^{54}Fe // Phys. Rev. C. 1989. V. 40. P. 559–569.

147. *Williams A. L. et al.* Gamow–Teller strength in $^{60,62,64}\mathrm{Ni}(n, p)$ reaction at 198 MeV // Phys. Rev. C. 1995. V. 51. P. 1144–1148.

148. *Yanka T.-H., Hillebrandt W.* Supernova neutrinos spectra // Astron. Astrophys. 1989. V. 224. P. 49–59.

149. *Walecka J. D.* Semi-leptonic weak interaction in nuclei // Muon Physics / Eds. V. W. Hughes, C. S. Wu. N. Y.: Academic, 1975. V. 2.

150. *Kuramoto T. et al.* Neutrino-induced reaction cross sections at intermediate energies for chlorine and water detectors // Nucl. Phys. A. 1990. V. 512. P. 711–736.

151. *Auerbach N., Van Giai N., Vorov O. K.* Neutrino scattering from ^{12}C and ^{16}O // Phys. Rev. C. 1997. V. 56. P. R2368–R2370;
Volpe C. et al. Microscopic theories of neutrino-^{12}C reactions // Phys. Rev. C. 2000. V. 62. P. 015501-1-3.

152. *Hayes A. C., Towner I. S.* Shell-model calculations of neutrino scattering from ^{12}C // Ibid. V. 65. P. 044603-1-3.

153. *Qian Y.-Z. et al.* Neutrino-induced neutron spallation and supernova r-process nucleosynthesis // Phys. Rev. C. 1997. V. 55. P. 1532–1544.

154. *Lutostansky Yu. S., Panov I. V.* // Proc. of Intern. Conf. «Low Energy Weak Interaction». Dubna, 1991. P. 148–152;
Nadyozhin D. K., Panov I. V., Blinnikov S. I. The neutrino-induced neutron source in helium shell and r-process nucleosynthesis // Astron. Astrophys. 1997. V. 335. P. 207–217.

155. *Guba V. G., Urin M. G., Nikolaev M. I.* Optical-shell-model approach to the GT excitations in nuclei // Sov. J. Nucl. Phys. A. 1990. V. 51. P. 622–631.

156. *Surman R., Engel J.* Neutrino caprure by r-process waiting nuclei // Phys. Rev. C. 1998. V. 58. P. 2526–2530.

157. *Fuller G. M., Meyer B. S.* Neutrino capture and supernova nucleosynthesis // Astrophys. J. 1995. V. 453. P. 792–809.

158. *Hektor A. et al.* Neutrino-induced reaction rates for r-process nuclei // Phys. Rev. C. 2000. V. 61. P. 055803-1-12.

159. *Engel J.* Approximate treatment of lepton distortion in charge-current neutrino scattering // Phys. Rev. C. 1998. V. 57. P. 2004–2009.

160. *Langanke K., Kolbe E.* Neutrino-induced charged-current reaction rates for r-process nuclei // At. Data Nucl. Data Tables. 2001. V. 79. P. 293–315.

161. *Antony M.* Coloumb displacement between analog levels for $3 < A < 239$ // At. Data Nucl. Data Tables. 1997. V. 66. P. 1–64.

162. *Pham K. et al.* Fragmentation and splitting of the GT resonances in $\mathrm{Sn}(^3\mathrm{He}, t)\mathrm{Sb}$ charge exchange reactions, $A = 112-124$ // Phys. Rev. C. 1995. V. 51. P. 526–540.

163. *Volpe C. et al.* Charged-current neutrino–^{208}Pb reactions // Phys. Rev. C. 2002. V. 65. P. 044603-1-5.

164. *Fuller G. M., Haxton W. C., McLaughlin G.* Prospects for detecting supernova neutrino flavor oscillations // Phys. Rev. D. 1999. V. 59. P. 085005-1-11.

165. *Austin S. M. et al.* Splitting of the dipole and spin-dipole resonances // Phys. Rev. 2001. V. 63. P. 03422-1-5.

166. *Kolbe E., Langanke K.* Role of ν-induced reactions on lead and iron in neutrino detectors // Phys. Rev. C. 2001. V. 63. P. 025802-1-11.

167. *Athanassopoulos C. (LSND Collab.)* // Phys. Rev. C. 1998. V. 54. P. 2489–2498.

168. *Eitel K., Zeinitz B. (KARMEN Collab.)* // Nucl. Phys. B. 1998. V. 77. P. 212.